J. Adhesion, 1999, Vol. 69, pp. 307–359
Reprints available directly from the publisher
Photocopying permitted by license only

Direct Observation of Cavitation and Fibrillation in a Probe Tack Experiment on Model Acrylic Pressure-Sensitive-Adhesives*

HAMED LAKROUT, PHILIPPE SERGOT and COSTANTINO CRETON†

Laboratoire de Physico-Chimie Structurale et Macromoléculaire, UMR 7615 du C.N.R.S, ESPCI, 10 Rue Vauquelin, 75231, Paris Cédex 05, France

(Received 1 May 1998; In final form 13 July 1998)

The adhesion mechanisms of two acrylic Pressure-Sensitive-Adhesives on a stainless steel probe are investigated with a custom-designed probe tack apparatus. Our setup allows the simultaneous acquisition of a nominal stress and strain curve, and the observation of the adhesive film from underneath the transparent substrate. The temperature was varied in the range −20°C to 50°C and the debonding rate in the range 1 – 10000 μm/s. For all conditions we observed, upon debonding, the formation of cavities at or near the interface between the probe and the film. These cavities initially grew predominantly in the plane of the film but, at higher values of nominal strain, the walls between the cavities were stretched in the direction normal to the plane of the ifim to become a fibrillar structure. The transition from a cavitated structure to a fibrillar one was only found within a time-temperature window of rheological properties of the adhesive, while the adhesion energy was found to be mainly related to the elongational properties of the adhesive. The maximum tensile stress observed in the probe tack experiment was directly related to the appearance of the cavities and showed a good correlation with the shear modulus of the adhesive, while the adhesion energy was found to be mainly related to the elongational properties of the adhesive. The presence of 2% acrylic acid as a comonomer had a negligible effect on the maximum stress but a very important one on the formation of a fibrillar structure and on the locus of failure.

Keywords: Tack; Pressure-Sensitive-Adhesive; acrylate; cavitation; fibrillation

*Presented at the 21st Annual Meeting of The Adhesion Society, Inc., Savannah, Georgia, USA, February 22-25 1998.

†Corresponding author. Tel.: +33 1 40794683, Fax: +33 1 40794686, e-mail: costantino.creton@espci.fr

I. INTRODUCTION

Usage properties of Pressure-Sensitive-Adhesives (PSA's) are usually characterized with three types of test: instant adhesion under light pressure, release force in a peel test and shear resistance. The probe tack test falls in the first type of test and is generally used to probe the instant adhesion properties of PSA's. The time of contact between the adhesive and the adherend can be specifically controlled and can be very short (well below one second). On the other hand, tack tests are generally not designed to probe the effect of very long contact times (hours or days).

Within those limits, Zosel has shown that the probe tack test can be used very effectively to gain some information on the mechanisms of debonding of the adhesive [1]. It provides some unique advantages in terms of controlling the experimental parameters. The applied compressive force, contact time and debonding rate can be easily independently controlled and the experiment can be done in a temperature-controlled chamber.

Therefore, while in principle the probe tack test was designed to test the short contact time-low pressure behavior, we have used it more as a tool to investigate the deformation behavior of soft adhesives in the general case. As opposed to the peel tests, where the peel angle and choice of backing can clearly influence the measured peel force, we expect that, in our probe tack test, the only parameters which will influence the results will be the rheological properties of the adhesive layer and the nature of its interactions with the two surfaces (that of the substrate and of the probe).

The optimum shape of the probe is an important question. While flat-ended probes are still the standard in industrial probe tack tests of PSA's [2], a recently-published industrial study argued that the spherical probe gives more reproducible results than the flat-ended probe [3]. While this particular argument is clearly correct (the use of a spherical probe circumvents the difficulty of a proper alignment between the probe and the film), the differences between the two geometries should be discussed a little further.

The choice of the optimum geometry depends on the type of adhesion which is investigated and the degree of detailed analysis which is desired from the data. Spherical cap probe tack testers indeed

have the advantage of avoiding alignment problems so that the strees distribution under the cap is very well controlled and can be easily reproduced. However, it is highly inhomogeneous within the adhesive film so that different parts of the adhesive are subjected to very different strain rates.

This inhomogeneous stress field always causes the debonding to start from the outside of the contact area. If the adhesive is a crosslinked elastomer which behaves macroscopically like a soft elastic solid, the contact problem can be treated mechanically with the so-called JKR approximation [4] provided that the finite size of the adhesive film is properly taken into account [5]. The mechanics of this type of crack propagation has been extensively studied experimentally and theoretically [6–8] and has been reviewed recently [5, 7]. This type of tack experiment yields very interesting data on the dynamics of crack propagation at an interface between viscoelastic materials and provides information on the relationship existing between the crack energy release rate, G, and the velocity at which the crack propagates [6, 9]. On a more microscopic level, the propagation of a crack in a viscoelastic medium has also recently been discussed theoretically [10–12].

However, the analysis becomes much more complicated when, as is typical for weakly-crosslinked or uncrosslinked PSA adhesives, large and inhomogeneous deformations occur in the adhesive layer. Therefore, for PSA testing, a spherical probe will indeed give a more reproducible fingerprint of the adhesive but will be ill-suited to more systematic investigations of the molecular parameters controlling the adhesion.

The use of a flat probe, on the other hand, gives a much more uniform stress field and strain rate under the probe surface and is better suited to the detailed investigation of very soft adhesives which will undergo cavitation and fibrillation processes when subjected to a tensile stress. From our experience, for soft adhesives (shear modulus below I Mpa) the alignment problem can be overcome and this point will be reconsidered in more detail in the discussion section of this paper.

In a previous publication, Creton and Leibler [13] investigated theoretically the necessary conditions to obtain good contact between a solid rough substrate and a soft adhesive. An important assumption

of that work was that the area of contact established during the bonding phase was directly proportional to the debonding energy. While some experimental results have been consistent with this model in a certain range of conditions [1, 14], the model does not provide useful predictions in the important regime where the area of contact is independent of contact time and pressure. In this case, it is important to know what are the main parameters controlling the maximum debonding stress, σ_{max}, and the adhesion energy, W_{adh}. Several authors have pointed out that the debonding of PSA's in peel tests or probe tack tests does not occur through the propagation of a crack at the interface between the adhesive and the substrate but, rather, through the formation of fibrils in the tensile direction which are progressively extended [15–17]. The plastic deformation of these fibrils in extension would then be the main energy-dissipating mechanism.

In the peel test geometry, Urahama [18] has shown that the crack propagates through the formation of Saffman–Taylor fingers, the precise shape of which depends on the adhesive and the substrate used. More recently, some elegant experiments [19–21] have shown that the stability of these fingers is controlled by the elongational properties of the adhesive as postulated some time ago by Good and Gupta [22].

In the probe tack geometry, where the adhesive is confined between two rigid parallel plates, Zosel has shown that good PSA's form (upon debonding) a fibrillar structure [16]. The molecular conditions necessary for its formation have been discussed by Zosel, who argued that a high molecular weight between entanglements, *i.e.*, a low plateau modulus, is a necessary condition for the formation of this fibrillar structure. A slight degree of branching and crosslinking is beneficial for the stability of the fibrils but excessive crosslinking can lead to a premature failure of the fibrils, therefore reducing significantly the adhesion energy [23, 24].

However, despite some significant theoretical efforts [10, 25], the detailed mechanisms by which this fibrillar structure forms are not yet clear. It is the purpose of this paper to investigate the early stages of fibril formation in a cavitating PSA. In a similar way to what has been done for the peel tests [17, 18, 20, 25, 26], such an investigation requires an observation tool which can give information on the deformation mechanisms of the adhesive in real time during the

debonding process. Zosel has shown that a side view of the probe can give a clear indication of the existence of the fibrils in the late stages of debonding. More importantly, he showed that the fibrils are observable optically and are, therefore, rather large in size (relative to a molecular size). However, a more quantitative analysis giving, for example, fibril size and spacing cannot be obtained from such a side view of a cylindrical probe as only the outside surface of the fibrillating structure is visible. A more useful observation viewpoint, from a quantitative analysis standpoint, is underneath the adhesive layer. If the substrate is transparent, the entire deformation process of the adhesive and, in particular, the early stages of fibril formation can be observed during the probe tack experiment and assigned to a specific point in the force-displacement curve. Therefore, it is possible, for a variety of experimental conditions, to have a detailed description of the mechanisms of deformation during the different stages of the debonding process.

For this purpose we used two model adhesives prepared from latices and which can be readily prepared as films.

II. EXPERIMENTAL

Materials

Our model Pressure-Sensitive-Adhesives (PSA) were:

- a random copolymer of a 98 wt% 2-ethylhexyl acrylate-2% acrylic acid (PEHA-AA) and
- a homopolymer of poly(2-ethylhexyl acrylate) (PEHA)

synthesized by emulsion polymerization and provided by Elf Atochem. The polymers do not contain additives other than a small amount of surfactants and have been obtained as latices with about 50% solid content. Given the presence of chains of very high molecular weights, possibly with a gel fraction, it was not possible to obtain a GPC characterization of the polymers. However, the DSC at a 10°C/min heating rate gave T_g's of -54°C and -50°C for PEHA and PEHA-AA, respectively.

Since the precise molecular characteristics of the polymers were difficult to obtain, it was important to have a characterization of their linear viscoelastic properties.

The master curves of the linear viscoelastic shear moduli, G′ and G″, at a reference temperature of 20°C for the PEHA and PEHA-AA are shown on Figure 1. The dynamic shear moduli obey time-temperature superposition and the shift factors, a_T, are reported in

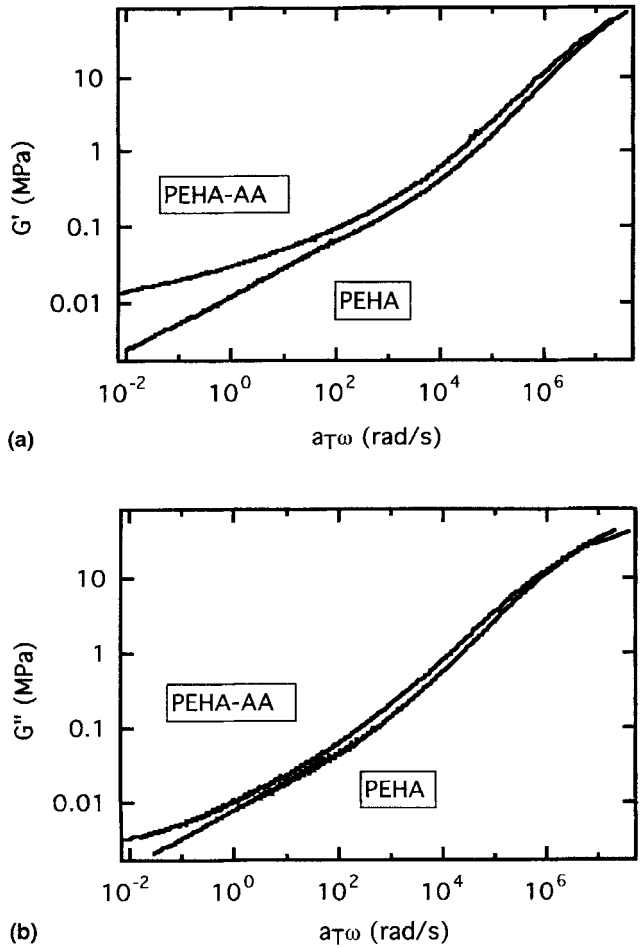

FIGURE 1 Master curves at a reference temperature of 20°C of the shear moduli (a) G' and (b) G'' *versus* $a_T\omega$ for the PEHA and the PEHA-AA.

Table I. The data fit the WLF equation relatively well in the temperature range investigated (−50°C to 50°C) and the WLF constants obtained from the fits at the respective glass transition temperatures are:

$$\text{PEHA: } C_1^g = 12.8;, C_2^g = 81.7°\text{C}$$
$$\text{PEHA-AA: } C_1^g = 12.2;\ C_2^g = 84.2°\text{C}$$

The values of C_2^g are a bit high relative to the universal constants but consistent with values found for poly(*n*-butylmethacrylate) and poly(2 ethyl-hexyl methacrylate) [27].

The absence of a plateau region is characteristic of a very wide distribution of molecular weights including some low molecular weight fractions and some very high molecular weights. Interestingly, there are only very minor differences in the shear moduli induced by the presence of the acrylic acid. The most notable difference is the higher value of G' for the PEHA-AA at the lowest frequencies. This result indicates the increase in the long relaxation times of the polymer and has been noticed by others [28]. In a way the acrylic acid groups act as additional physical crosslinks with very long relaxation times. On the other hand, both DSC and rheometry indicate that the T_g is virtually unaffected by the presence of acrylic acid.

Furthermore, the shear moduli of the polymers at room temperature and 1 Hz are relatively low, around 10^4 Pa, indicating the very

TABLE I Rheological shift factors, a_T, for the PEHA and PEHA-AA polymers obtained from a Rheometrics parallel plate rheometer. The reference temperature is 20°C and the same shift factors are used also for the adhesion master curves

Temperature (°C)	*log a_T (PEHA)*	*log a_T (PEHA-AA)*
−50	5.64	5.62
−40	4.22	4.25
−30	3.11	3.18
−20	2.27	2.30
−10	1.55	1.58
0	0.98	0.98
10	0.50	0.46
20	0	0
30	−0.42	−0.42
40	−0.85	−0.76
50	−0.99	−1.07

compliant nature of these model PSA's relative to a typical rubber-based PSA.

Probe Tack Experiment

The samples are made by depositing a small amount of latex on a glass microscope slide and then doctor-blading it to a film of uniform thickness. The thickness of the film varied somewhat from sample to sample but was kept at approximately 70 μm and was precisely measured for each sample. After depositing the film on the slide, the sample was dried first in air at room temperature and then for 4 hours at 70°C under vacuum. Given the nature of the latices from which these samples are prepared, the surface was not molecularly smooth. The average roughness of the films was characterized by its average asperity size, $R_a = (1/L) \int_0^L |z| dx$, as measured by optical interference microscopy, where $|z|$ and L are defined on Figure 2a. An optical photograph of the dried film surface giving a value of $R_a = 0.1$ μm is shown on Figure 2b. The characteristic wavy texture of the film due to the coalescence of the latex particles is evident. The probe used in this investigations was a cylindrical stainless steel probe with a diameter of 1 cm and a randomly-rough surface obtained by sanding with 50 μm diameter alumina particles. The average height of the asperities was characterized with a mechanical profilometer and was $R_a = 1.2$ μm. The distribution of asperity heights was approximately Gaussian. This sanding process was done to create a surface of uniform characteristics. In some experiments we also used a machined stainless steel surface ($R_a = 0.1$ μm), and a polished glass surface ($R_a = 0.05$ μm).

The probe tack experiment was done on a custom-designed apparatus adapted on a MTS 810 hydraulic testing machine schematically shown on Figure 3a. The sample is fixed on the upper plate which is connected to the load cell. The parallelism between the sample and the probe is controlled through three micrometer screws which can finely adjust the position of the upper plate as described on Figure 3b. The probe is fixed on the mobile lower shaft and its displacement is controlled with an LVDT transducer. The entire setup is enclosed in a temperature-controlled chamber. If the sample is properly illuminated with a fiber optic light source, the entire process of contact between the probe and the film and the subsequent

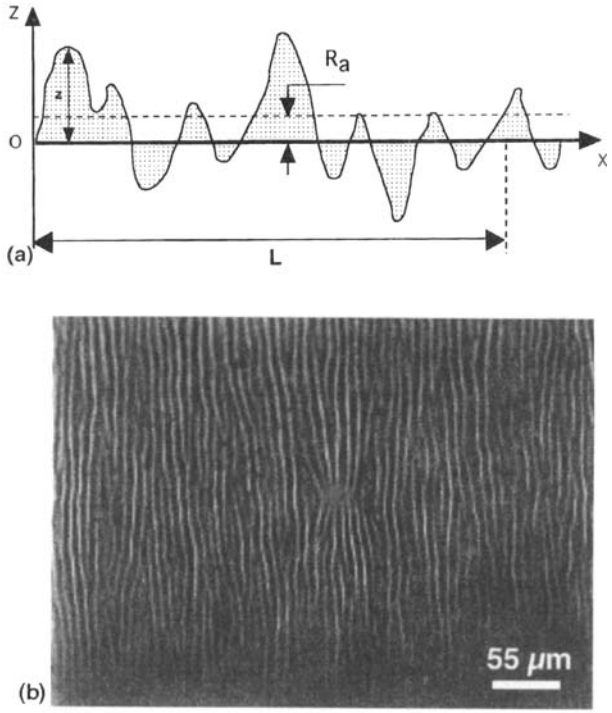

FIGURE 2 (a) Schematics of a rough surface showing the important geometrical parameters defined in the text which are used for its characterization; (b) Optical micrographs of the surface of a dried film of PEHA. The surface has been previously coated with a thin layer of gold to improve the contrast.

debonding can be followed from under the glass slide with a 45-degree mirror and a video camera placed outside the temperature chamber. The displacement resolution of our instrument is of the order of 1 μm while the force resolution is approximately 0.2 N. An interesting characteristic of this setup is the very high rigidity of the assembly which has a compliance of 0.3 μm/N including the bending of the glass slide. Furthermore, the compliance can be easily measured and subtracted from the experimental curve so that the stress–strain curves actually reflect the deformation of the adhesive only.

The tests were performed in the following manner: The probe was brought into contact with the film at a constant crosshead speed of 30 μm/s. As soon as the desired compressive force was achieved, the displacement was kept constant therefore allowing the force to relax

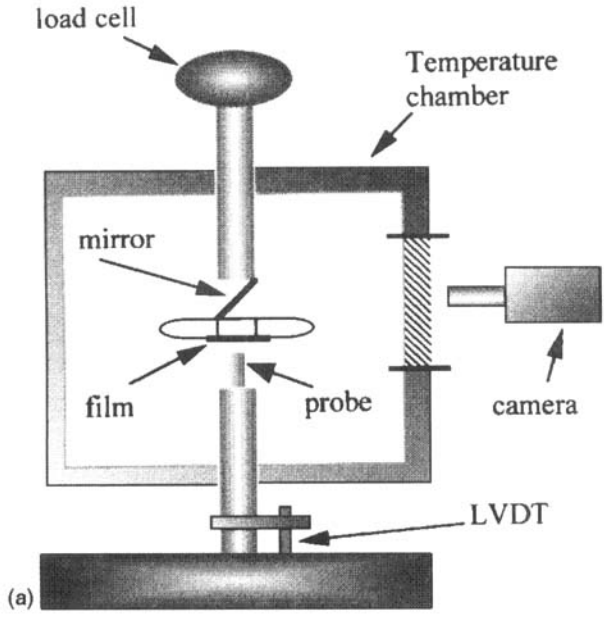

FIGURE 3 (a) Overall schematics of the probe tack apparatus and (b) Detailed schematics of the upper plate showing the adjustment of the parallelism between the probe and the glass slide.

during the specified contact time. This experimental procedure is slightly different from the Polyken^{TM} probe tack experiment where the compressive force is kept constant and the indentation of the probe in the adhesive increases with contact time. Although this difference might affect the contact time dependence of the adhesion energy, we feel that in the regime where adhesion is not contact limited (which is most of the results of this study) our experimental procedure does not significantly affect the debonding mechanisms.

Unless specified otherwise, the applied compressive force was 78.5 N (corresponding to 1 MPa nominal contact pressure for a full contact area) and the contact time was 1 second. The probe was then removed from the film at a constant crosshead speed which was varied between 1 and 10000 μm/s. The temperature of the chamber was varied between −20°C and 50°C. During each experiment, the force, the displacement of the crosshead and the time were acquired simultaneously. A typical force and displacement plot as a function of time is given in Figure 4.

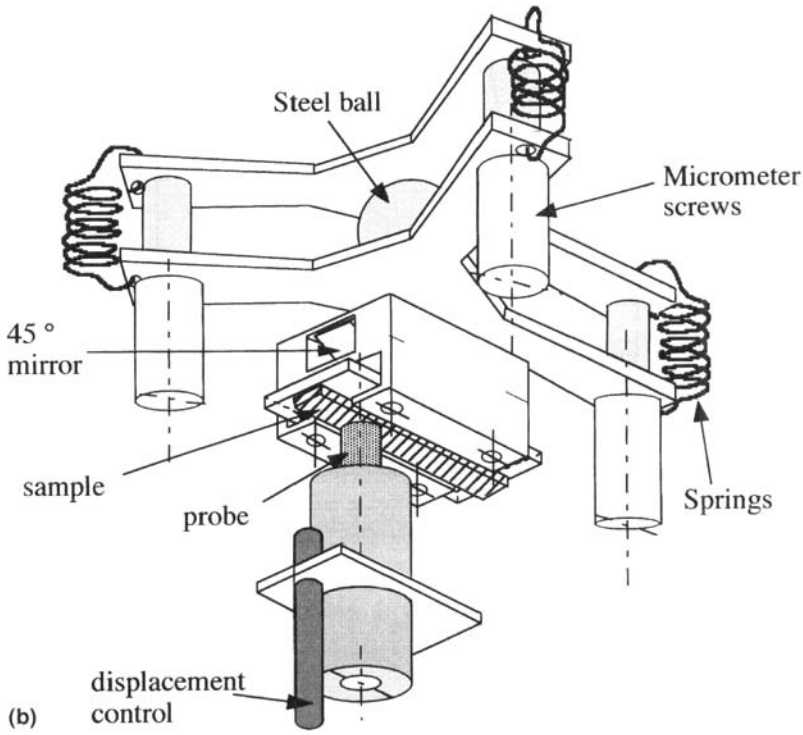

FIGURE 3 (Continued).

The tests were filmed with a black and white CCD camera and recorded on a VCR. Selected images were then digitized and analyzed. Several types of information were typically obtained from the digitized images:

(1) The time at which a first contact between the probe and the film was observed. This time was used to synchronize the subsequent images with the stress–strain curves. Since the standard European video captures 24 frames/sec, the uncertainty on the time was about 40 ms.
(2) The real macroscopic contact area between the probe and the film (despite the alignment of the probe with the film, the area of contact was usually not 100% of the surface of the probe as shown on Fig. 5). We do not, however, have any information on the possible presence of trapped air in submicronic pockets.

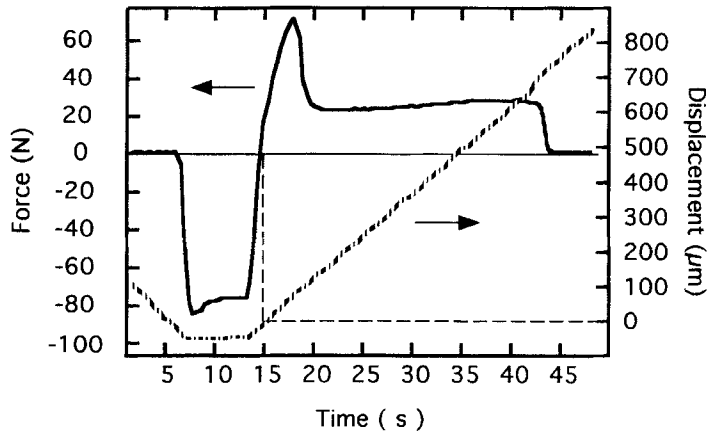

FIGURE 4 Typical force (———) and displacement (— - — -) curves as a function of time.

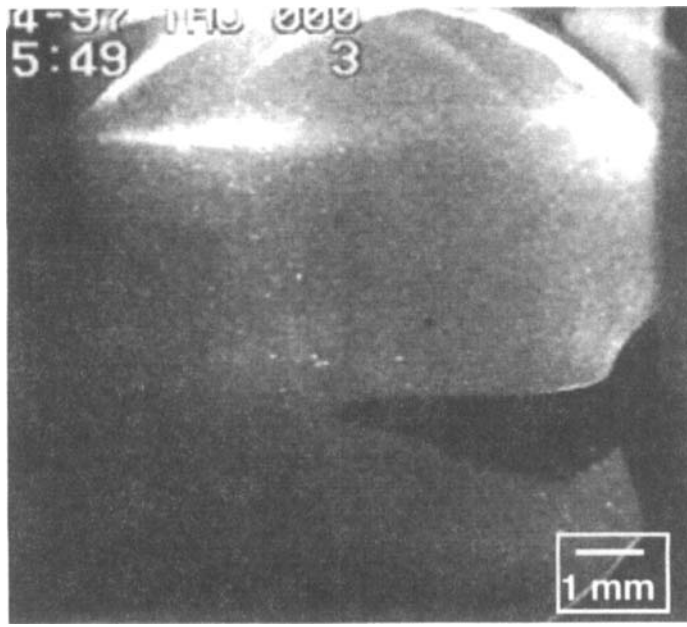

FIGURE 5 The surface of the probe which is in contact with the film during the compression stage is in lighter color. Note that not all of the surface of the probe is in contact with the film. This is due to a macroscopic waviness of the probe surface.

(3) In the debonding stages, the kinetics of cavity formation and growth as projected in the plane of the film.

The force signal was renormalized by the real area of contact (obtained from the video) to give the nominal compressive and tensile stress on the film and the displacement signal was renormalized by the initial thickness of the film to give a nominal strain. One should bear in mind, however, that these values have the meaning of true stress and strain only in the regime where the deformation of the film is homogeneous.

The rheological experiments were performed on a Rheometrics RDA II parallel-plate rheometer and the samples were prepared by drying approximately 2 grams of the latex to a pellet and then depositing the pellet between the two 8 mm diameter plates of the rheometer. The pellet was then squeezed to a disk in the rheometer and the shear measurements were made.

III. RESULTS

The instrumented probe tack experiment that we have developed provides a substantial amount of information for each test. In order to present the results in a clear and comprehensible way, we have organized the results section in the following way:

In Section III.1 we present a typical experimental curve with some video captures and define the various experimental quantities which are then compared, in the following sections, for the two acrylate polymers. The Sections III.2 to III.5 present the results obtained in our "standard" conditions (1 second contact time and I MPa nominal compressive pressure on the rough steel probe) as a function of temperature and debonding rate. They are analyzed in various degrees of detail:

In Section III.2 we will present the conventional analysis of probe tack results which considers the maximum stress measured during the debonding stage (σ_{max}) and the integral under the stress–strain curve, sometimes called Zosel tack, which we will refer to as the adhesion energy (W_{adh}). In Section III.3 we will consider the additional information provided by the analysis of the shape of the stress–strain

curve and of the locus of failure (cohesive, glass/polymer interface, probe/polymer interface). Finally, in Section III.4 we will present the additional results provided by the video observation of the debonding process.

In Sections III.5 and III.6 we will present some preliminary results obtained by varying the contact time on the rough metal probe and by changing the probe surface at fixed contact time. More extensive results on the effect of these two parameters will be presented in a forthcoming paper but we feel that these preliminary results provide useful insights to understand the debonding mechanisms.

III.1. Typical Experimental Results Obtained from a Test

From each experiment, we obtained a curve showing the nominal stress *vs.* nominal strain. We could then extract a maximum debonding stress, σ_{max}, generally called "Tack" in the standardized ASTM probe tack test [29], and a total adhesion energy, W_{adh}, as proposed by Zosel and defined in Figure 6.

While this analysis of the stress–strain curves is essential to obtain a quantitative evaluation of the performance of the adhesive, it provides only limited information on the detailed mechanisms of debonding. In order to gain a better understanding of these mechanisms we need to couple the video observation of the bonding and debonding process to the stress–strain curve.

As an example of the additional information provided by the video camera, a typical sequence of images is shown on Figure 6, for a sample tested at 25°C and at a debonding rate of 10 μm/s. For each frame, the position on the simultaneously-acquired stress–strain curve is also shown. The gray area in the frames shows the fraction of the area of the probe which is in contact with the film.

The different stages of the debonding process can described as follows:

(a) Homogeneous deformation of the film in tension. In this regime the force increases rapidly with displacement and there are no voids optically visible. This stage is not shown on Figure 6 and corresponds to the initial increase in the tensile stress.
(b) Nucleation and rapid growth of macroscopic voids at the probe-film interface. The voids nucleate first in the region which was last

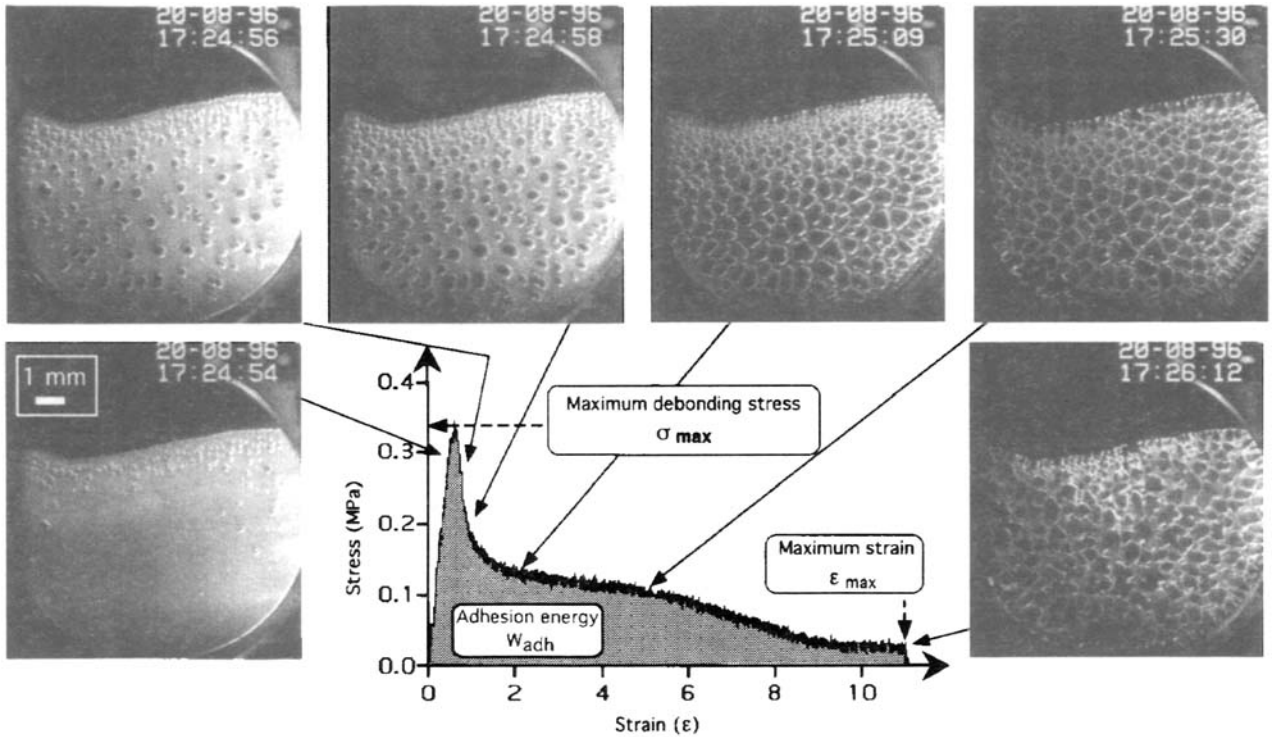

FIGURE 6 Typical stress–strain curve obtained from a probe tack test showing the maximum stress, σ_{max}, the maximum extension, ε_{max}, and the integrated adhesion energy, W_{adh} (shaded area). The video captures show the different stages of the debonding process as observed from underneath the glass slide.

brought in contact with the probe and then relatively homogeneously over the whole contact surface. This mechanism occurs near the maximum in the measured nominal stress. The void nucleation is shown on images 1 through 3 on Figure 6.

(c) Slower growth of these voids until most of the initial contact area is occupied by the voids. Note that, for our materials and experimental conditions, the growth of the voids stops short of the coalescence. As observed from underneath, the structure looks like a foam. During this regime the nominal stress decreases markedly and stabilizes. This regime is mostly seen in the change between images 3 and 4 of Figure 6.

(d) No further change is visible from underneath but the walls of the foam will elongate in the direction of the applied stress at an approximately constant level of nominal stress. Images 4 and 5 of Figure 6 show the initial and final image of that stage.

(e) Air penetrates the voids and the walls between the cells are broken forming isolated fibrils which eventually debond from the probe (adhesive failure) or break (cohesive failure). During this stage the nominal stress decreases slowly to zero. Image 6 is typical of the end of this stage.

III.2. Maximum Stress and Adhesion Energy

As mentioned previously, the standardized analysis of a probe tack experiment provides the user with a single value: that of the maximum stress, σ_{max}. However, in the case where extensive fibrillar debonding takes place, the adhesion energy, W_{adh}, might be a better way to characterize the "tack" of a particular adhesive [30]. We have plotted on Figures 7 and 8 σ_{max} and W_{adh} for both polymers as a function of debonding rate at different temperatures. Both tack parameters show an increase with increasing debonding rate over most of the range of parameters investigated. This behavior is consistent with other studies [31] and can be attributed to the viscoelastic losses occurring in the adhesive layer which should increase with increasing deformation rate of the adhesive layer.

The effect of temperature, on the other hand, is more complicated, since the change in temperature will affect both the kinetics of bonding

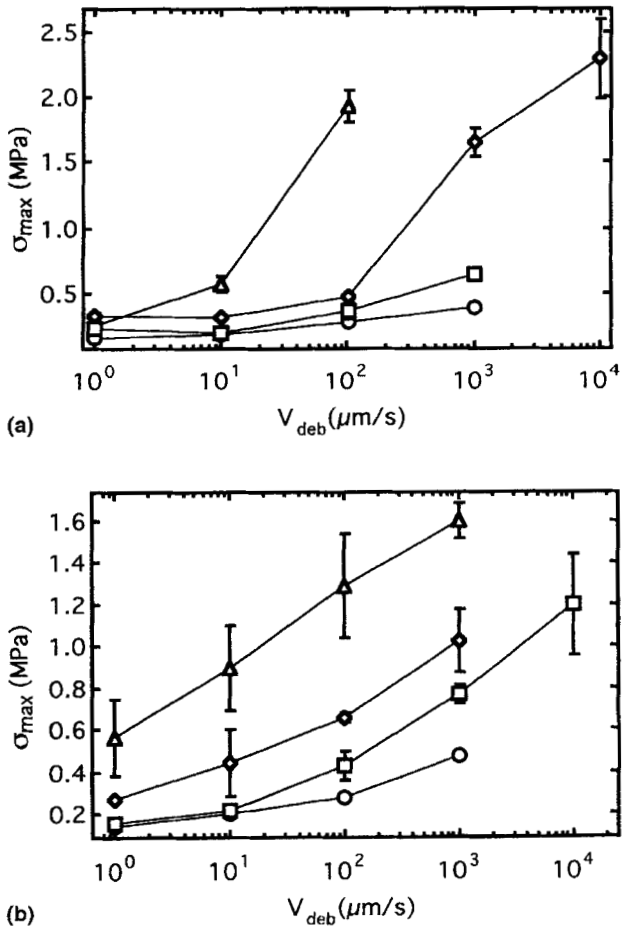

FIGURE 7 Maximum debonding stress, σ_{max}, as a function of debonding rate at different temperatures (–○– 50°C, –□– 20°C, –◇– 0°C, –△– –20°C) for (a) PEHA and (b) PEHA-AA.

and the debonding process. A typical PSA tested in probe tack shows a maximum of adhesion energy for a temperature of 50 to 70°C above its T_g [30]. The existence of a maximum in dissipated energy at a temperature much higher than the glass transition temperature was first attributed to an incomplete contact between the probe and the surface during the short contact time. This incomplete contact would

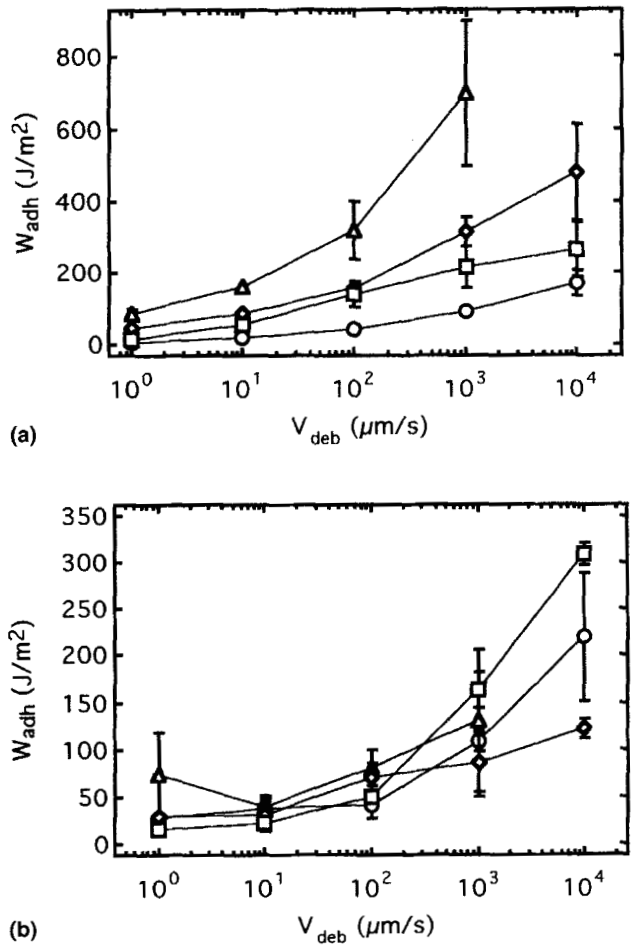

FIGURE 8 Adhesion energy, W_{adh}, as a function of debonding rate at different temperatures (–○– 50°C, –□– 20°C, –◇– 0°C, –△– –20°C) for (a) PEHA and (b) PEHA-AA as a function of debonding rate.

only occur at the lower temperatures, therefore decreasing the real contact area between the probe and the film. A more quantitative theoretical treatment of this effect has also recently been published [13]. However, in a more recent paper, Zosel argues [24] that this effect could also be due to the stability of the fibrillar structure which cannot

form below a certain temperature. Our findings tend to support this hypothesis.

As shown on Figure 9a, the temperature dependence of σ_{max} is similar for both polymers and for both debonding rates. For the contact time of 1 second σ_{max} increases monotonically with decreasing temperature. However, if one considers W_{adh} (Fig. 9b) the PEHA and

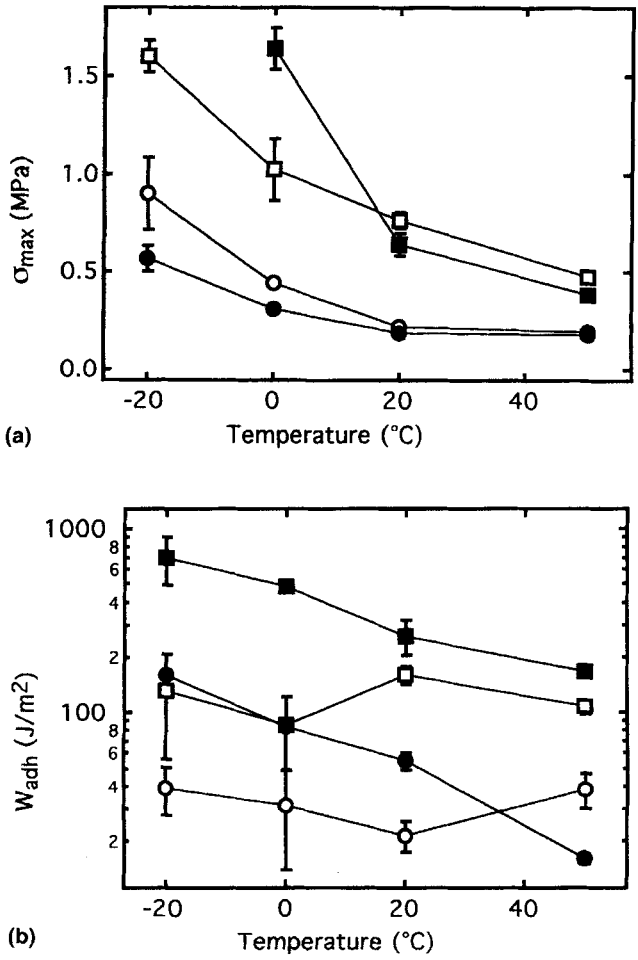

FIGURE 9 (a) σ_{max} and (b) W_{adh} as a function of temperature for PEHA and PEHA-AA *at two different debonding speeds* (PEHA: -●- 10 μm/s, -■- 1000 μm/s; PEHA-AA: -○- 10 μm/s, -□- 1000 μm/s).

PEHA-AA show qualitatively a different behavior. For both debonding rates W_{adh} is nearly independent of temperature for the PEHA-AA, while it increases monotonically with decreasing temperatures for the PEHA. If an insufficient contact was responsible for the behavior of the PEHA-AA, one would expect the maximum stress to be equally affected. Since this is not the case it is more likely that the difference in the temperature dependence of W_{adh} for the two adhesives is due to a different debonding micromechanism.

III.3. Shape of the Stress–Strain Curve and Locus of Failure

A better insight into the differences in the debonding mechanisms can be obtained by a careful analysis of the shape of the stress–strain curves coupled with the examination of the locus of failure (*i.e.*, adhesive at the probe/film interface, cohesive or adhesive at the glass/film interface).

As a first illustration, it is interesting to see how the stress–strain curve typically evolves when the debonding rate and temperature are changed. Figures 10 and 11 show, for the PEHA, the effect of debonding rate at 50°C and the effect of temperature at the nominal debonding rate of 10 μm/s. It is interesting to note that while the value

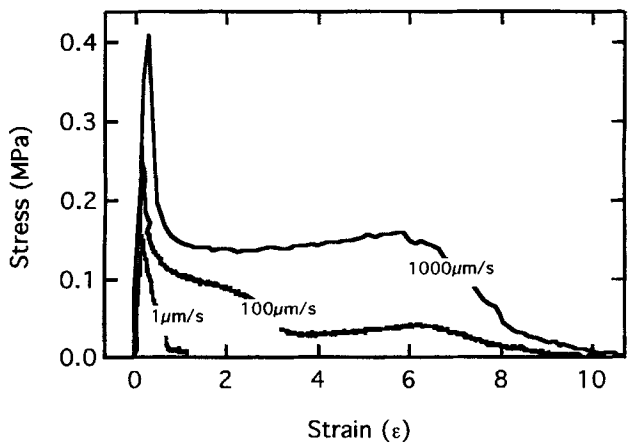

FIGURE 10 Effect of the debonding rate on the stress–strain curves for PEHA at a fixed temperature of 50°C.

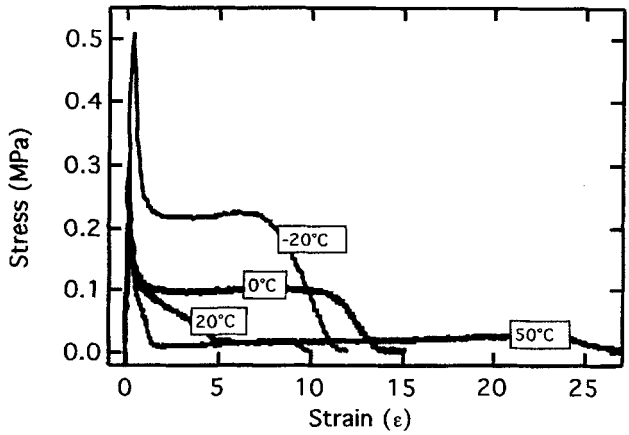

FIGURE 11 Effect of the temperature on the stress–strain curves for PEHA at a fixed debonding rate of 10 μm/s.

of the maximum stress and of the debonding energy change in a monotonic way, reflecting the results presented on Figures 7 and 8, the shape of the curve changes, suggesting the existence of transitions in the debonding mechanisms.

Although in some cases we are in an intermediate regime, the nominal stress–strain curves which we observed can generally fit relatively well within five categories, schematically defined on Figure 12. The Type I curve occurs at high temperatures and low debonding rates for the PEHA only. It is characterized by a linear decrease of the stress to zero after the maximum and a small maximum extension.

The Type II curve occurs at low rates of debonding and intermediate temperatures for the PEHA-AA polymer mainly. Relative to the Type I curves, a change in slope occurs during the decrease of the stress to zero but no plateau stress is observed.

The Type III curve occurs at low to intermediate rates of debonding and high temperatures. In this case the stress decreases to a plateau value after the maximum and then, at a given value of the extension, a typical dip in stress is observed and a second plateau, at lower values of stress, is observed until final fracture occurs. The maximum extension is typically very large in this case but the plateau stress is low.

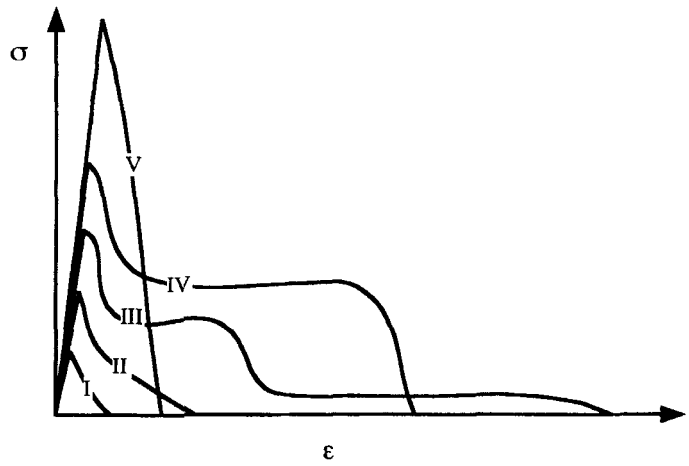

FIGURE 12 (a) Schematics of the five different Types (I to V) of stress–strain curves described in the text.

Type IV curves are typical of a fibrillar failure and occur at high debonding rates (except at the lowest temperatures). In this case the stress decreases to a plateau value which then remains nearly constant until the stress decreases to zero. The plateau value is typically higher than for Type III curves and the extension is high. This is the type of curve the results in the maximum debonding energy.

Finally, Type V curves are seen at low temperatures and high debonding rates and are typical of a "brittle" fracture. In this case the stress decreases almost instantaneously to zero after the maximum. The maximum stress is often high but the extension is very low.

An important usage property of a commercial pressure-sensitive adhesive is the ability to debond from the substrate without leaving much residue. In other terms, with our experimental geometry, an adhesive debonding from the probe is highly desirable. Although we did not perform any surface analysis which could have given molecular information on the locus of fracture, the experiments could be classified according to a macroscopic locus of fracture criterion, *i.e.*, cohesive, adhesive at the glass/polymer interface or adhesive at the probe/polymer interface.

Figure 13 shows a map of the types of curves, observed experimentally, for PEHA and PEHA-AA while Figure 14 shows a fracture

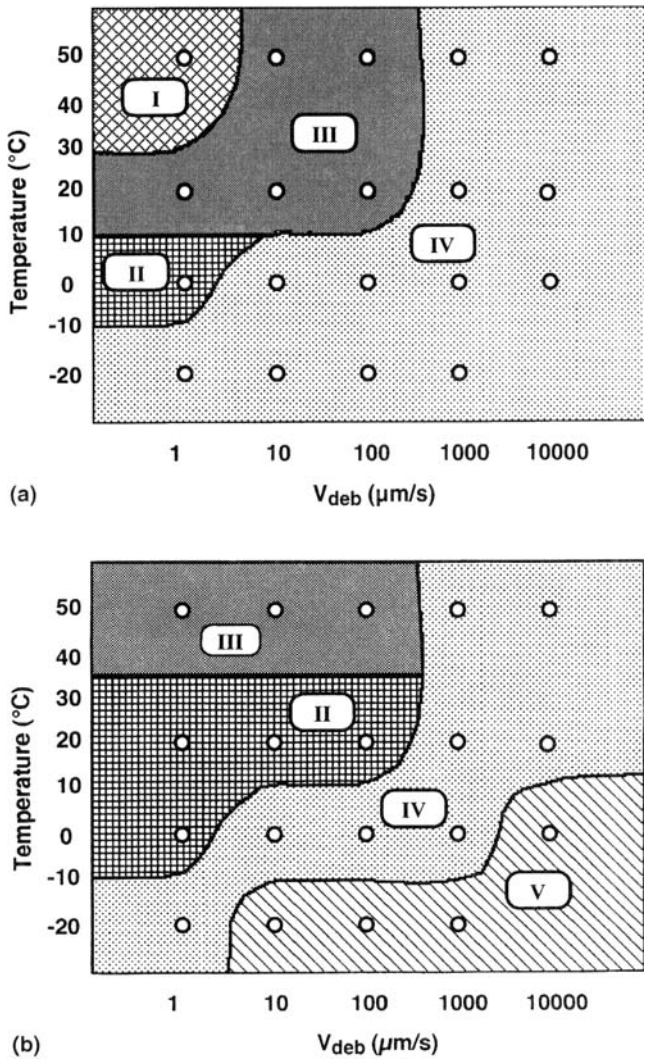

FIGURE 13 Map of the different types of curves observed as a function of temperature and debonding rates for (a) PEHA and (b) PEHA-AA. The circles represent the actual rates and temperatures of our tests.

mechanisms map of the locus of fracture for different experimental conditions for both polymers. Clearly, the presence of the acrylic acid does qualitatively shift the mechanisms of failure towards higher temperatures and lower debonding rates.

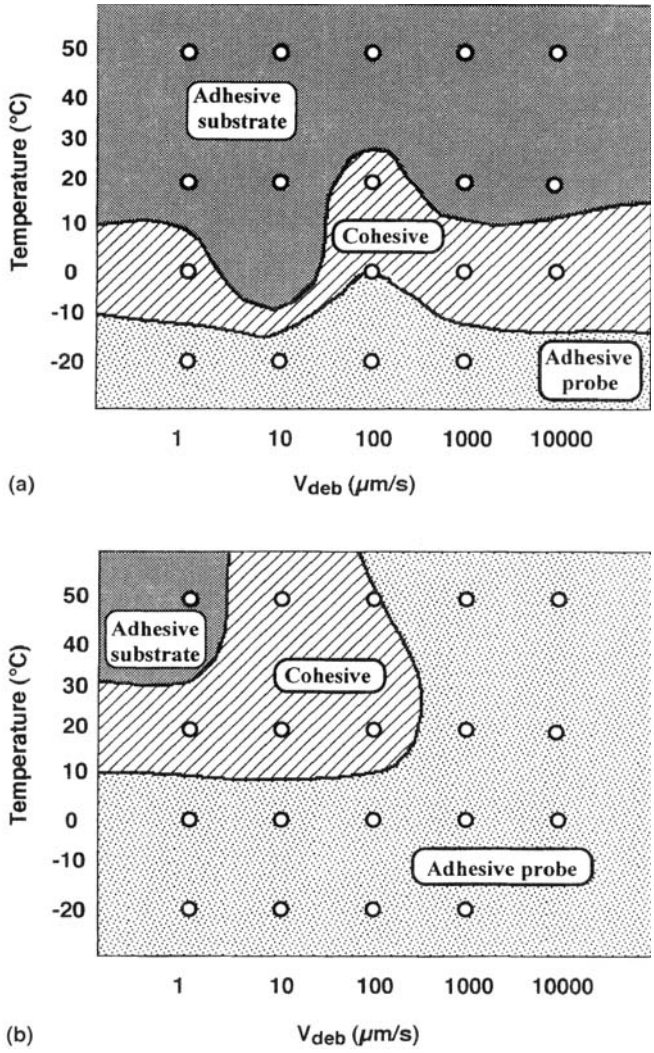

FIGURE 14 Map of the locus of failure as a function of debonding rate and temperature for (a) PEHA and (b) PEHA-AA. The circles represent the actual rates and temperatures of our tests.

Two apparently surprising results have been observed.

(1) The presence of acrylic acid has a very marked effect on the locus of failure and this effect is not very intuitive. The presence of AA increases the tendency of the polymer to fail at the probe/polymer

interface, while one would expect the AA to increase the favorable interactions with the probe. The reason for such a behavior is discussed in Section IV and lies in the modifications introduced by the AA group on the *bulk* as well as on the *interfacial* properties of the polymer [28, 32]. For those relatively short contact times, the change in bulk properties controls the behavior since the diffusion of acrylic acid to the polar metal surface can be very slow.

(2) Even more surprisingly, the locus of failure of the PEHA polymer changes from adhesive/probe to cohesive to adhesive/glass by increasing the temperature, implying apparently a significant change of the interfacial interactions with temperature. We will argue in Section IV that this change in locus of failure can be completely rationalized by a change in the rheological properties of the PEHA with temperature and does not imply a change in interfacial interactions with temperature.

An additional insight can be obtained by separating the contribution of the nucleation and growth of the cavities (the area under the initial peak) from the contribution due to the fibrillar growth in the direction perpendicular to the plane of the film (the area under the shoulder) as described schematically on Figure 15a. If the fraction of W_{adh} due to the growth of fibrils is plotted as a function of $a_T V$ (Fig. 15b), the transition from a debonding mechanism involving fibrillar growth and one which does not, becomes more evident. For PEHAAA this transition occurs for $a_T V > 10^4$ and for PEHA it occurs for $a_T V < 10$. For the PEHA-AA the high $a_T V$ behavior corresponds to the Type V curves, *i.e.*, brittle fracture, and for the PEHA, the low $a_T V$ behavior corresponds to the Type I curves, *i.e.*, a liquid like behavior where dewetting occurs.

III.4. Growth of the Cavities and Final Size

The analysis of the video images captured during debonding provided important help in the interpretation of the stress–strain curves in terms of mechanisms. A first important observation was that, in all cases, the maximum in stress was related to the formation of cavities in the polymer film. Some experiments performed at a higher magnification, where the small depth of focus of the lens allowed one to

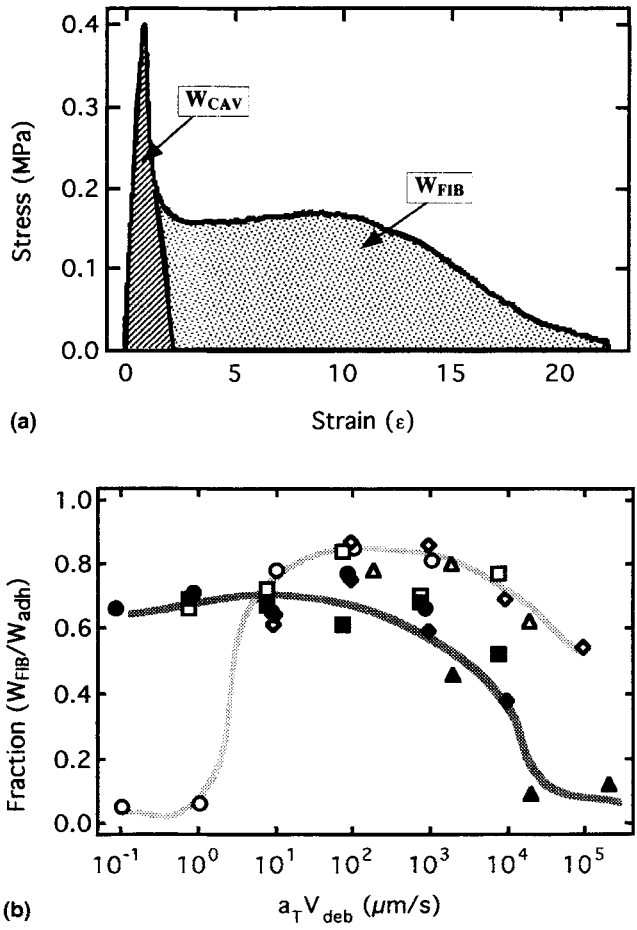

FIGURE 15 Schematics showing the energy, W_{CAV}, dissipated during the cavitation process and the energy, W_{FIB}, dissipated during the fibrillation process; (b) Fraction of the total adhesion energy which is dissipated in the fibrillar growth (W_{FIB}/W_{adh}) for PEHA (*unfilled symbols*) and PEHA-AA (*filled symbols*) as a function of $a_T V$ at a reference temperature of 20°C. (–○– 50°C, –□– 20°C, –◇– 0°C, –△– –20°C). The thick line is a guide to the eye (▒ PEHA, ■ PEHA-AA).

discriminate between the surface and the bulk, revealed that the cavities always nucleated at, or very near, the probe/film interface, and could be assimilated to interfacial cracks. The first cavities always occurred before the maximum in stress and were responsible for a nonlinear increase in stress. At the maximum, however, the nucleation

became widespread and most of the surface was covered with the cavities. An interesting experimental observation was that the cavities appeared randomly on the surface and not first at the center of the probe surface. This result, which has never been reported before, implies that, in this very confined geometry, the negative hydrostatic stress is fairly homogeneous under the probe surface. Further implications of this observation will be discussed in Section IV.

Except for the Type V curves, the decrease in stress corresponded to the growth of the cavities in the plane of the film, as shown on Figure 6, until the walls between them reached a critical size. At this point, the rest of the debonding mechanism was strongly dependent on the adhesive and on the temperature and debonding rate and gave rise to very different stress–strain curves.

For Type I curves, the cavities observed had a pronounced non-spherical shape and an example is shown on Figure 16A. While one would have expected for these conditions a cohesive fracture within the walls between the cavities, the observed locus of failure in this case was always adhesive at the glass/film interface as shown on the locus of fracture maps of Figure 14. Furthermore, no fibrillar structure was formed.

For Type II curves, the situation was almost identical except for the fact that the cavities retained a spherical shape and were relatively small as shown on Figure 16C. In this case however a limited amount of fibrillar structure was formed but no distinct shoulder was observed. The locus of fracture was always cohesive. For Type III curves (Fig. 16B), the walls between the cavities no longer rapidly fail by disentanglement upon elongation but form a honeycomb structure with cells elongated in the tensile direction. It should be pointed out at this point that there probably is a significant pressure difference between the inside and the outside of the cavities, which have grown essentially from submicronic air pockets. The very thin walls between the cells will then yield to the outside pressure and the air will penetrate inside. This process, readily observable on the video, appeared to cause a dip in stress and a double plateau curve as shown on Figure 10 for the debonding rate of 100 μm/s. The second plateau at very low stress reflects the elongation of thin separated fibrils. This type of curve occurs only at the higher temperatures and results either in a cohesive fracture or in an adhesive fracture at the glass interface.

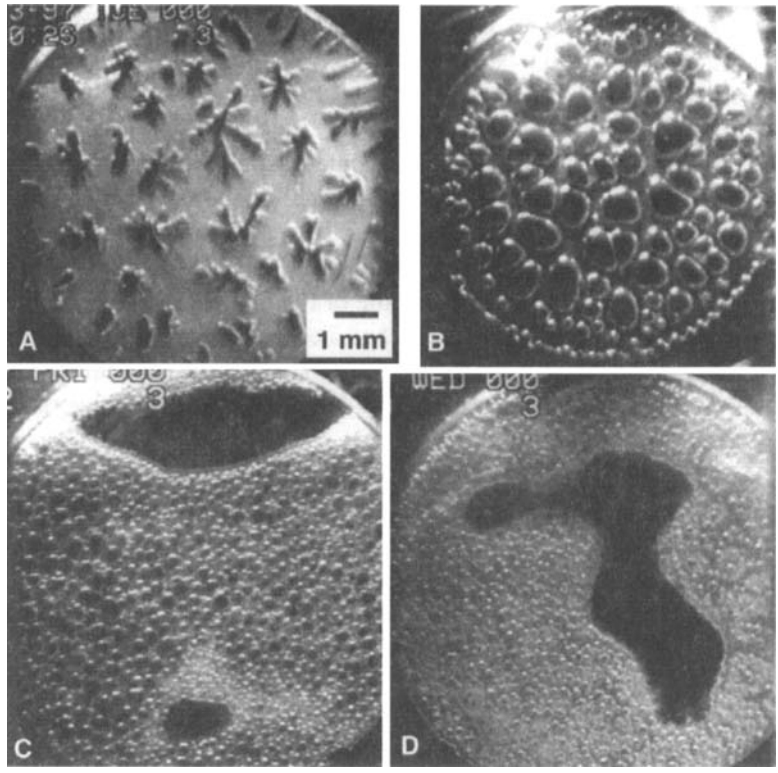

FIGURE 16 Images of late stages of debonding: (A) Dendritic cavities observed for the PEHA at 1 μm/s and 20°C or 50°C (Type I curves); (B) Large spherical cavities typically observed for the PEHA at 20 and 50°C and V > 1 μm/s (Type III curves); (C) Small cavities observed for nearly all conditions for the PEHA-AA and for the PEHA at low temperature (Type II and Type IV curves) and (D) very small cavities observed during the "brittle" fracture of PEHA-AA at −20°C (Type V curves).

On the other hand, if the walls were sufficiently strong to resist the air pressure, the air penetration occurred simultaneously with the failure of the fibrils and a characteristic single plateau shape was observed. In this regime all three loci of fracture were observed. Finally, one should say a word about the Type V brittle fracture curves. Even for this type of curve, the formation of cavities was always observed, as shown on Figure 16D, but no fibrillar structure was formed. Rather, the initial cavities coalesced into a larger interfacial crack causing the macroscopic failure.

A statistical analysis of the video images provided some further information on the characteristic size of the cavities. Generally, these cavities were fairly homogeneous in size and evenly distributed on the surface of the probe. They eventually completely paved the surface so that it was possible to measure the projection of the average final area of the cavities in the plane of the film. The average final cavity area (projected in the plane of the film) as a function of debonding rate and for different temperatures, is shown on Figure 17 for both polymers. For the PEHA at the two higher temperatures, a marked rate dependence was observed with a general trend towards larger cavities with decreasing debonding rate. However, for the lower temperatures for the PEHA and at almost all temperatures for the PEHA-AA, the final size of the cavities could not be simply related to the rheological properties of the polymers but was rather constant. Interestingly, the cavity size was consistently smaller for the PEHA-AA polymer.

The shape of the cavities was almost always nearly spherical except for the PEHA at 50°C and V_{deb} = 1 μm/s. In this case, a characteristic dendritic shape of the cavities was observed. Typical late stages cavity images are shown for several conditions on Figure 16.

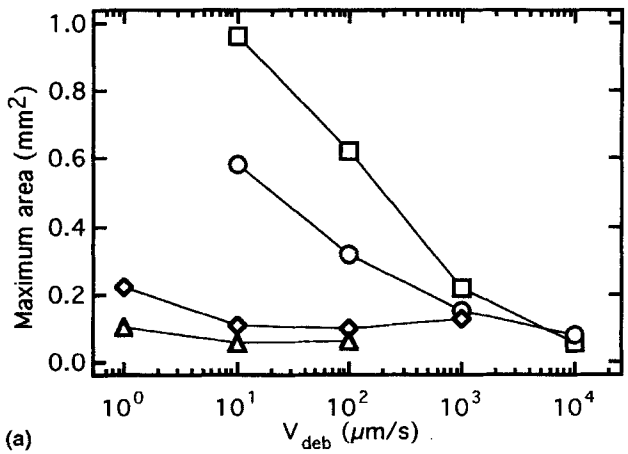

FIGURE 17 Maximum average area of a cavity, projected in the plane of the film, as a function of debonding rate at different temperatures (-○- 50°C, -□- 20°C, -◇- 0°C, -△- −20°C) for (a) PEHA and (b) PEHA-AA.

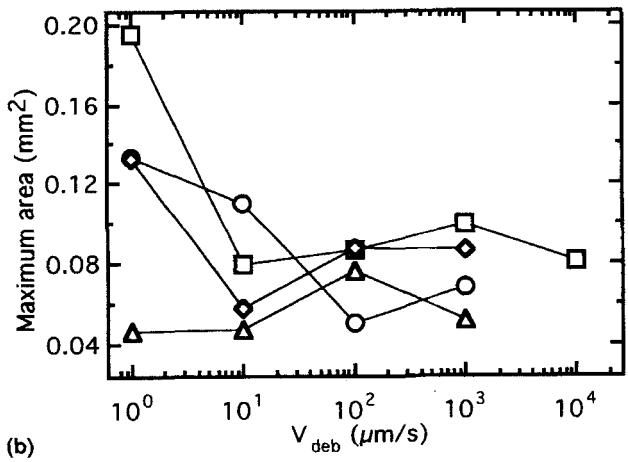

FIGURE 17 (Continued).

III.5. Effect of the Time of Contact

While the effect of the time of contact was not the initial goal of the study, we felt that it was important to be aware of the temperature where the cavitation stress or the adhesion energy are strongly influenced by the time of contact. Therefore, we show on Figure 18 stress–strain curves obtained at 0.1 s, 1 s and 60 s contact time at 50°C and at −10°C for the PEHA-AA polymer at a debonding rate of 10 μm/s. While at 50°C the contact time seems to have a negligible effect on the debonding mechanisms (the difference between the curves is within experimental error), one can see a large effect, particularly on the fibrillation part of the curve, at −10°C.

In our experiments we chose a contact time of 1 s since this value is generally used as a standard for probe tack experiments. While at the two higher temperatures we do not expect that a longer contact time would have modified our results, it should be borne in mind that, particularly for the temperature of −20°C, our experimental values are probably in the contact-limited regime. This dependence of the time of contact introduces an additional time parameter and we would expect the simple time-temperature superposition principle applied to the debonding rate/temperature variable pair to fail in the regime where adhesion depends on contact time.

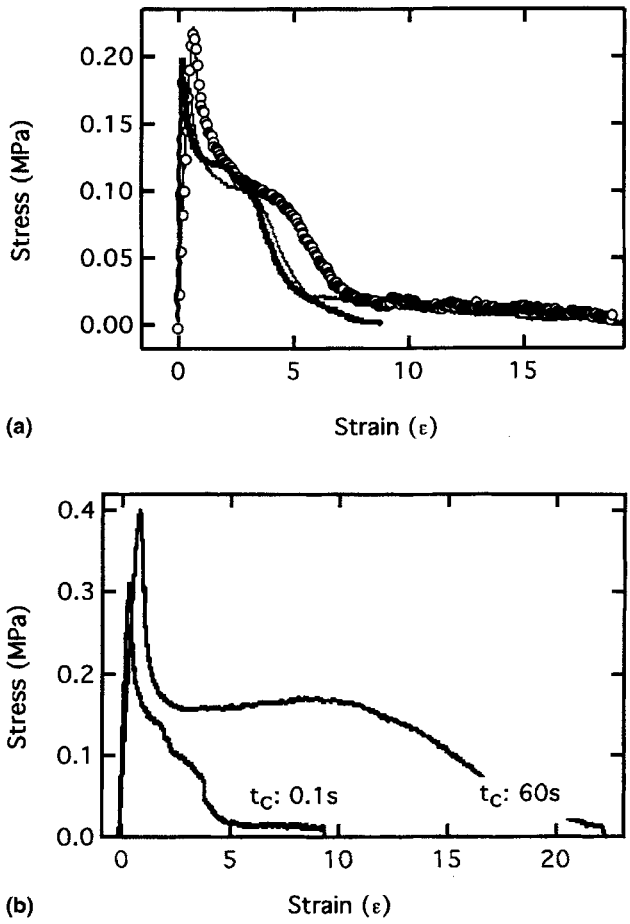

FIGURE 18 Stress–strain curves obtained at: (a) 0.1 s (–○–), ls (▬) and 60s (—) contact time at 50°C and (b) 0.1 s and 60s contact time at −10°C for the PEHA-AA polymer at a debonding rate of 10 μm/s.

III.6. Effect of the Probe Surface

In all our experiments we used the same probe surface, *i.e.*, a sanded stainless steel surface with an average roughness of 1.2 μm. However, we did perform some experiments with modified probes to gain some understanding on the relevance of the nature of the probe surface to the adhesion mechanisms. We tried a machined metal probe (R_a = 0.1 μm) and a polished glass probe (R_a = 0.05 μm). Further more, we

also deposited on the metal probe a thin (0.5 μm) layer of polystyrene and used this modified probe as our surface. Some typical stress–strain curves are shown on Figure 19a, for $T = 50°C$ and a debonding rate of 10 μm/s. The following trends were observed: The maximum stress increased significantly when going from a rough probe to a smooth one; on the other hand, the polished glass probe behaved very similarly to the polished metal one. The polystyrene-coated probe gave a maximum stress in between that of the smooth and of the rough steel. More striking differences were observed in the morphology of the debonded area as shown on Figure 19b. Clearly, there is a

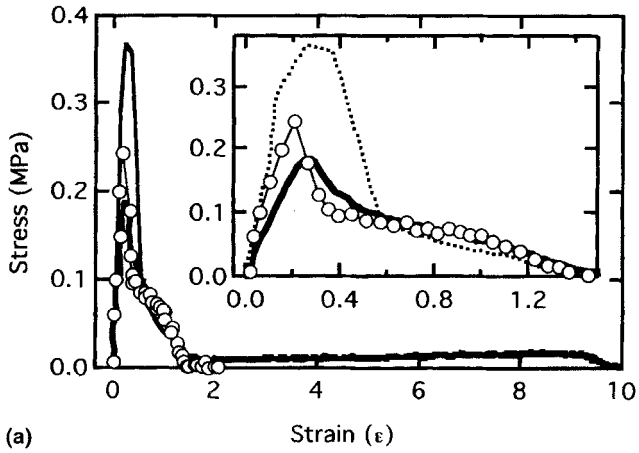

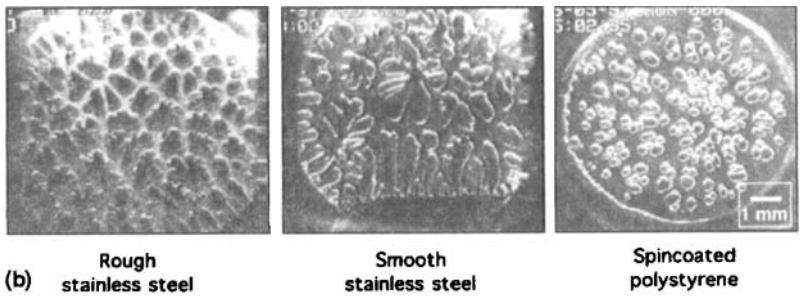

FIGURE 19 (a) Stress–strain curves for the PEHA at a debonding rate of 100 μm/s and at 20°C on different probe surfaces: polished metal (- - - -), spincoated polystyrene (-○-), rough metal (▬). The region of the peaks is zoomed in the inset; (b) Corresponding video images of the debonding patterns on rough metal, polished metal and polystyrene.

significant amount of coupling between the surface properties of the probe and the bulk properties of the adhesive and the pattern of nucleation and growth of the cavities (before fibrillation occurs) is quite sensitive to it. For these experimental conditions, only the rough probe gave a significant fibrillar structure (and at a low value of stress). All the other surfaces did not evolve into a fibrillar structure so that, in the end, the respective values of W_{adh} were all quite comparable, for the smooth surfaces at about 10–12 J/m^2 and the rough steel was somewhat higher at 16 J/m^2. Therefore, a superficial analysis of the role of the surface could have concluded to a minor effect for the wrong reasons.

IV. DISCUSSION

In view of the results presented in Section III, we can develop a tentative model of the mechanisms controlling the tack of these soft polymers and emphasize the salient differences resulting from the presence of the acrylic acid.

IV.1. Time-temperature Superposition

An important point in the analysis of the adhesion of soft polymers is to consider more quantitatively the relevance of the time-temperature superposition principle. Since we were interested in testing the correlation of the rheological measurements with the adhesion measurements, we constructed on Figures 20 and 21 an adhesion master curve for the maximum stress and for the adhesion energy using the shift factors, a_T, obtained from the linear viscoelastic measurements of G' and G'' shown on Figure 1.

The t-T superposition appears to work well for both adhesives if the maximum stress is taken as the main parameter, and this was regardless of the type of stress–strain curve experimentally observed.

However, if the main parameter is now the adhesion energy, the t-T superposition works reasonably well for the PEHA adhesive, although in a less convincing way than for the maximum stress, but clearly fails to predict the behavior of the PEHA-AA adhesive. The failure of the t-T superposition for the PEHA-AA adhesive at the lower temperatures

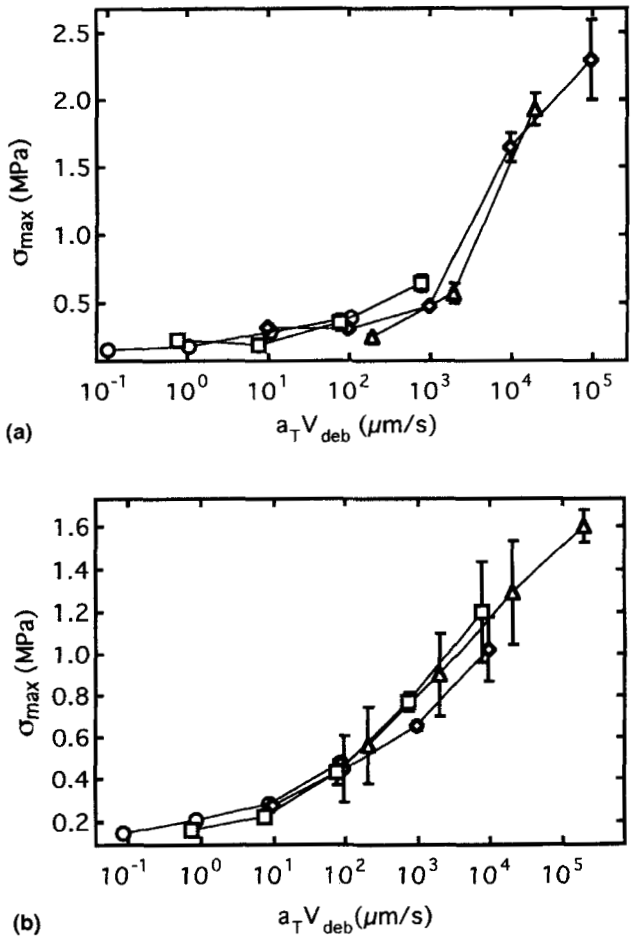

FIGURE 20 σ_{adh} as a function of $a_T V$ at a reference temperature of 20°C for (a) PEHA and (b) PEHA-AA (-○- 50°C, -□- 20°C, -◇- 0°C, -△- -20°C).

is not in principle surprising, since in Section III.5 we have presented evidence that the debonding behavior of the PEHA-AA is dependent on the time of contact at the lower temperatures. However, it is interesting to note that a short contact time appears to have a dramatic effect on the formation of a fibrillar structure (reflected by the value of the adhesion energy) but not on the maximum stress which still obeys rather well the t-T superposition.

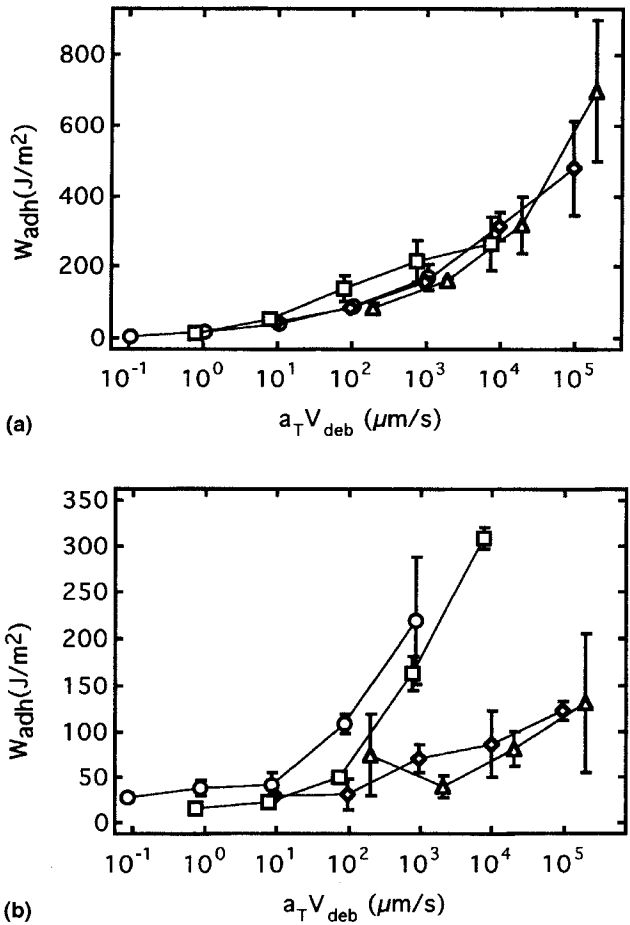

FIGURE 21 W_{adh} function of $a_T V$ at a reference temperature of 20°C for (a) PEHA and (b) PEHA-AA (–○– 50°C, –□– 20°C, –◇– 0°C, –△– –20°C).

One could argue, alternatively, that the nucleation and growth of the cavities which controls the maximum stress is mainly dependent on the shear properties of the adhesive and is, therefore, well predicted by a measurement of the linear viscoelastic shear modulus. However, a large contribution to the adhesion energy comes from the formation of a fibrillar structure which is presumably sensitive to the non-linear elongational viscoelastic properties of the adhesive. These properties cannot be directly predicted from shear properties. Preliminary

investigations on the elongational properties of PEHA and PEHA-AA have shown that the presence of acrylic acid reduces significantly the ability of the polymer to undergo large extension ratios.

IV.2. Nucleation of Cavities

Clearly, the probe tack geometry introduces a very strong hydrostatic component in the stress field and that hydrostatic component is responsible for the extensive cavitation which is observed. The question is, then, to relate the process of nucleation and growth of these cavities to the rheological properties of the adhesive, to the surface properties of the adherend and, if possible, to the molecular characteristics of the polymer.

A more quantitative modeling of the cavitation process is beyond the scope of this paper and the reader is referred to the pioneering work of Kaelble [25] and Gent [33, 34] for a more detailed discussion. However, several remarks can be formulated:

The mechanical behavior of a thin rubber cylinder between two rigid plates, as schematically described on Figure 22a, has been investigated and reviewed recently [35–37]. A crucial point controlling the behavior of these films is the degree of compressibility of the polymer as given by its bulk modulus, K. For a fully incompressible polymer, the hydrostatic pressure, p, at the center of the thin layer can be approximated by [35]:

$$p = E\varepsilon\left(\frac{a^2 - r^2}{h^2}\right) \tag{1}$$

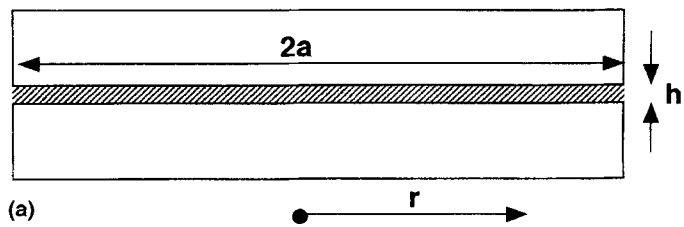

FIGURE 22 (a) Schematics of the confined adhesive layer of thickness h between two plates of radius a; (b) Hydrostatic pressure distribution (normalized by the average pressure) in the middle of the adhesive layer as a function of the normalized radius r/a. The calculations are done for our typical experimental conditions, *i.e.*, $a/h = 50$.

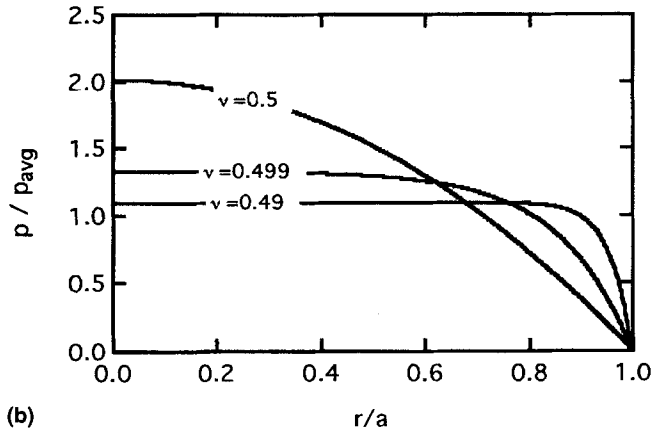

FIGURE 22 (Continued).

where a is the diameter of the cylinder, E is Young's modulus, ε is the applied strain in the tensile direction and h is the thickness of the layer.

Therefore, for $a/h = 50$, one expects a parabolic pressure distribution with a maximum in the center of the probe. On the other hand, for a nearly incompressible material (as given by a Poisson's ratio $v = 0.49$), the pressure distribution changes markedly and becomes much flatter. Its detailed shape can be calculated by a finite element method as a function of two adimensional parameters: a/h and the Poisson's ratio, v. The hydrostatic stress in the center of the film (normalized by the average pressure over the whole probe surface) is shown on Figure 22b for three different values of the Poisson's ratio. It is interesting to note that, for these very constrained experimental geometries, a small deviation from incompressibility will modify very markedly the stress distribution and have important effects on the debonding mechanisms. In particular, since the pressure gradient rapidly becomes very small when one goes towards the center of the probe, one does not expect the formation of Saffman–Taylor finger instabilities, which typically occur on thicker samples with a flat probe or in geometries such as the spherical probe or a peel test.

Gent and coworkers [33, 34, 38] have observed that the cavitation stress of crosslinked rubbers was directly related to their shear moduli rather than to their bulk moduli. In simpler terms, they predicted and observed experimentally that a rubber could not sustain a hydrostatic

stress which greatly exceeded its shear modulus without the growth of voids inside its structure. The argument rests on a purely elastic argument of the growth of an existing cavity in an elastic medium. Regardless of its size, the cavity is predicted to grow if [33, 34]:

$$\sigma > \frac{5E}{6} \tag{2}$$

where E is the Young's modulus of the rubber. An important point to note is that if the initial cavity is sufficiently large, the surface tension of the polymer or the interfacial tension with the substrate should not play any role in the expansion criterion. This critical size can be fairly small ($\sim$1 μm) for very viscoelastic polymer melts and defects of that size are readily found at the interface between a melt and a solid due to the very long relaxation times of the melt.

Equation (2) can be readily extended to a polymer melt by replacing the modulus, E, by a dynamic quantity, $G'(\omega)$. In this case, one expects the critical cavitation stress to be proportional to G' at a given frequency. Provided a suitable equivalence between $G'(\omega)$ and $\sigma_{cav}(d\varepsilon/dt)$ is found, one can directly compare the two quantities. In our experiments it is difficult to estimate directly the critical stress at which the first cavity forms, since this occurs before the maximum in stress and will be very sensitive to a slight misalignment between the probe and the surface. However, one can reasonably assume that, for a given probe surface and a given adhesive, the observed maximum stress is proportional to the cavitation stress since this maximum stress corresponds to the widespread nucleation of cavities over most of the probe surface.

Such a comparison between $\sigma_{max}((d\varepsilon/dt)a_T)$ and $G'(\omega a_T)$ is done on Figures 23a and b for the two polymers. While the equivalence criterion is somewhat arbitrary (we assumed that a frequency of $g = \bar{\omega} = 1$ Hz was equivalent to an initial strain rate of $d\varepsilon/dt = 1\ s^{-1}$), several observations can be made.

(1) For both polymers, $\sigma_{max} = 10\ G'$ in a certain range of frequencies. Although this result is not quantitatively compatible with Eq. (2), it is qualitatively correct. It should be noted that a very similar analysis has been made by Kaelble on peel test results [25]. In this case, he found that the cavitation stress followed well Eq. (2).

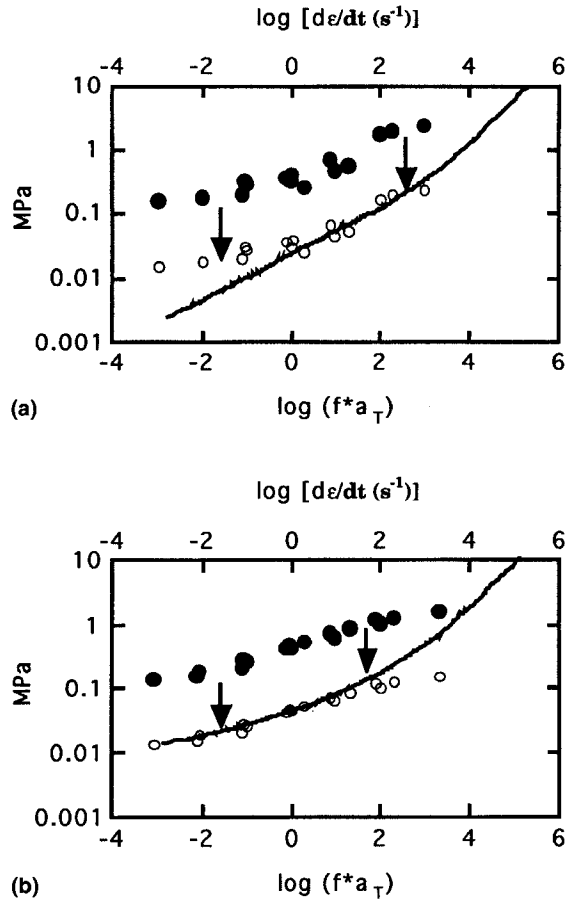

FIGURE 23 Comparison between the shear storage modulus, G' $(a_T g)$ (−) and maximum stress, $\sigma_{max}(d\varepsilon/dt)$ for (a) PEHA and (b) PEHA-AA. The correspondence between $a_T f$ and $d\varepsilon/dt$ was set based on reasonable assumptions explained in the text. The filled symbols represent the actual value of σ_{max} while the unfilled symbols are the best fit to the shear modulus data ($\sigma_{max} = 10\ G'$ for both PEHA and PEHA-AA).

(2) For the PEHA-AA adhesive the correlation between the shear modulus, G', and the maximum stress is good over the whole range of investigated frequencies. For the more liquid-like PEHA, on the other hand, the correlation is less good at low frequencies suggesting that, in that regime, a different parameter controls the maximum stress.

Interestingly, the experimental conditions where σ_{max} appears to have a different dependence on G' are the same as those where we observe important variations of the final diameter of the cavities (see Fig. 17).

Given the fact that the nucleation of cavities was always observed at the interface between the probe and the film, an important question is, then, the role of the surface in the nucleation of these voids, which, in the initial stages of growth, can be assimilated to interfacial penny-shaped cracks. The preliminary observations on the effect of the probe surface described in Section III.6 strongly suggest that both maximum stress and fibrillation process are affected by the nature of the surface. In view of these results, one can draw the following tentative picture of the initial stages of debonding:

The experimentally-measured force on the probe can be written as:

$$F(t) = \sigma(t)A(t) \tag{3}$$

where σ is the tensile stress and A is the load-bearing area. Before the cavities appear, σ increases with t and A remains constant. However, as soon as cavities appear both parameters change with time. At the maximum force measured experimentally, the following equation must be satisfied:

$$\frac{dF}{dt} = \sigma(t)\frac{dA}{dt} + A(t)\frac{d\sigma}{dt} = 0 \tag{4}$$

where the first term represents the decrease in load-bearing area and is negative and the second term is the increase in stress due to the applied tensile strain. An exact modeling of the time dependence of these quantities is difficult but one can formulate the following remarks:

- The second term is always positive until a yielding phenomenon (or a steady state flow) occurs.
- The first term is negative, as soon as cavitation appears, and has two contributions; the contribution due to the nucleation of new cavities and the contribution due to the growth of existing ones.

While the first contribution should be primarily related to the bulk properties of the adhesive as argued in the preceding paragraphs, the

second contribution should be related to the propagation of an interfacial crack between a hard solid and a viscoelastic one. In this case, the critical tensile stress for crack propagation, σ_{prop}, should scale as:

$$\sigma_{prop} \propto \left(\frac{\mathbf{G_c} G'}{c}\right)^{1/2} \tag{5}$$

where $\mathbf{G_c}$ is the critical strain energy release rate for the interfacial crack, G is the shear modulus and c is the radius of the crack.

IV.3. Growth of Cavities

Gent's model predicts infinite expansion of the cavity above this critical stress. However, this model pertains to the expansion of a cavity in an infinite elastic medium. This may be true at the initial stages of cavitation where the cavities do not "see" each other and nucleate independently on defects, but clearly fails to describe the observations made at later stages where a different formalism is needed.

Our observations clearly show that after a rapid growth the cavity stabilizes and then grows in a stable manner at fixed-grips conditions, *i.e.*, if the crosshead is stopped the cavity no longer grows. (Note that this behavior is no longer true for PEHA at the higher temperature). This behavior can be, at least approximately, described by a fracture mechanics approach.

Let us first consider the propagation of an annular crack in the elastic case. The stable growth of the cavities at fixed grips can be explained by the finite thickness of the polymer film. At the interface between a rigid punch of radius a and an infinitely thick elastic layer, an annular interfacial crack is always growing in an unstable manner, which essentially means that the driving force for crack propagation increases with increasing crack size. Therefore, once the applied energy release rate $\mathbf{G} > \mathbf{G_c}$, an increase in crack length causes $\mathbf{G}$ to increase and the crack to accelerate until catastrophic failure occurs. However, for an elastic layer of thickness comparable with a, the crack can grow in a stable manner at fixed grips within a range of values of a/h [39]. Although our materials are viscoelastic and we do not have a single annular crack propagating but several circular cracks propagating

simultaneously, the effect of the finite size should be similar and, by analogy, the radius a would be one-half the distance between two adjacent interfacial cracks and h, the thickness of the layer.

It is now worthwhile to take a look at the kinetics of crack growth in our viscoelastic material: As shown on Figure 24a, the cavities can be modeled as penny-shaped interfacial cracks growing between the probe and the polymer film, which behaves like a viscoelastic material. Therefore, when the displacement of the crosshead increases, the tensile stress, σ_{zz}, close to the crack increases and, in fracture mechanics terms, the applied **G** increases. Similarly, the hydrostatic pressure, p, in the elastic layer grows. However, while the tensile stress is maximum at the crack tip, the hydrostatic pressure will be maximum in between the two cracks as shown on Figure 24a. In a purely elastic material, this situation can either cause the crack to grow (if $\mathbf{G} > \mathbf{G_0}$) or the higher level of hydrostatic negative pressure between the two cavities can cause the nucleation of an additional cavity. Now, when a crack propagates at the interface between a solid surface and a viscoelastic one, an applied $\mathbf{G} > \mathbf{G_0}$ will cause the crack to propagate at a given velocity, $\dot{a}$, *i.e.*, one can define $\mathbf{G}(\dot{a})$ [6].

The occurrence of crack propagation or of cavity nucleation is controlled, then, by the dependence of the interfacial dissipative mechanisms on crack velocity. If the **G** *vs.* $\dot{a}$ curve is very flat as shown in the Case II of Figure 24b, a small increase in **G** (caused by the displacement of the crosshead) will immediately cause the crack to grow rapidly to the new equilibrium value. It becomes more difficult, then, to nucleate a new cavity.

If, on the other hand, the **G** *vs.* $\dot{a}$ curve is very steep, as in Case I of Figure 24b, the same increase in **G** will only cause a slow propagation of the crack and the level of hydrostatic pressure between cracks can then exceed the cavitation stress and a new cavity can nucleate.

Therefore, one expects that when the propagation is difficult (steep **G** *vs.* $\dot{a}$ curve), a large number of small cavities will be observed and the decrease in load-bearing area will be mainly controlled by the nucleation of new voids. The maximum stress should then be directly proportional to the elastic modulus of the adhesive. However, if the propagation of the interfacial cracks is easier (flat **G** *vs.* $\dot{a}$ curve) the maximum stress is presumably controlled by the interface. One expects to observe larger cavities and a maximum stress which is no longer

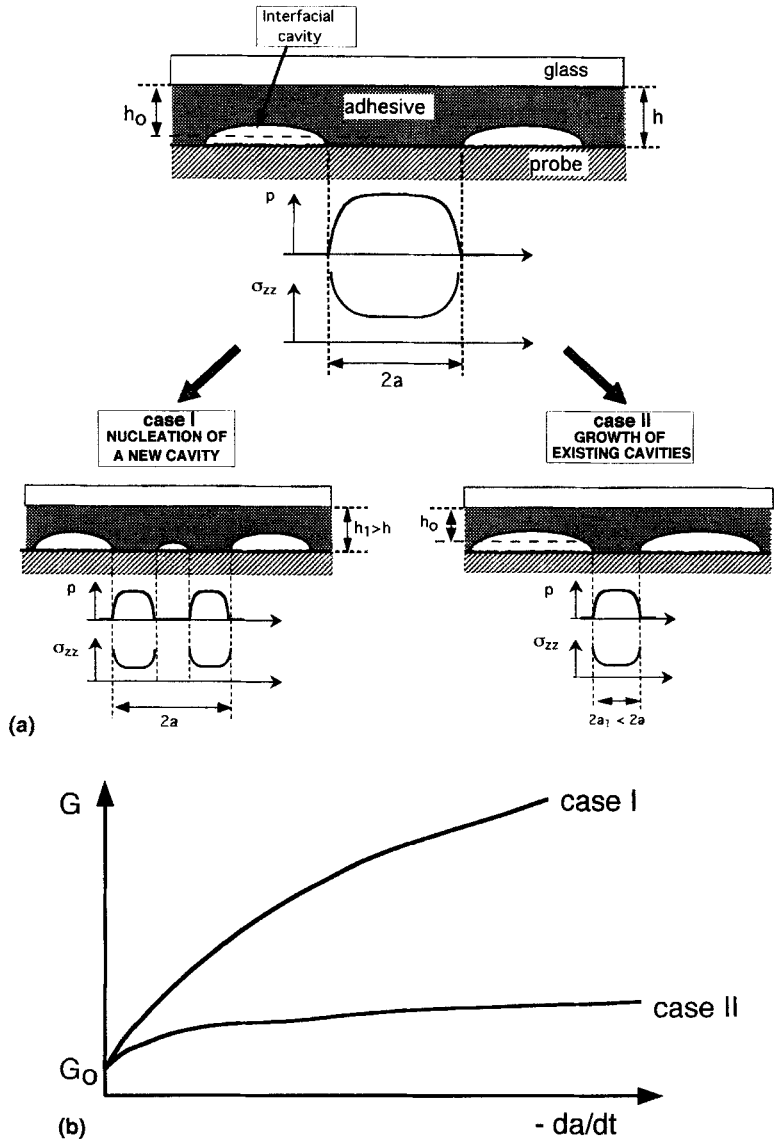

FIGURE 24 (a) Schematics of the nucleation of a new cavity in between two existing ones (Case I) and of the growth of two existing cavities (Case II); (b) Corresponding G *vs.* V curves of an interfacial crack for the two cases. The insets show schematically the hydrostatic pressure and the normal stress distribution at the interface between the film and the probe. Note that the maximum normal stress is at the crack tip while the maximum pressure is in between the two cavities.

directly proportional to the elastic modulus of the adhesive. This appears to be the case for the PEHA at high temperature as shown on Figures 17a and 23a.

Based on this interpretation, the role of the acrylic acid in the determination of the size of the cavities appears to be to increase the slope of the **G** *vs.* $\dot{a}$ curve, favoring the nucleation of a large number of cavities. Since we only observe the resulting dynamic effect, it is difficult to conclude whether the acrylic acid causes an increased interaction between the film and the surface (a higher G_0) or whether the PEHA-AA simply causes more interfacial dissipation in the sense described by Shull *et al.* [5].

An important effect which is not taken into account in this description is the shape of the crack opening. The cracks drawn on Figure 24 imply a propagation at a fixed contact angle of 90°, independently of the thermodynamic work of adhesion. In reality, the contact angle will be affected by the nature of the surface and will, in turn, affect the local stress field. However, we feel that our description captures the qualitative features of the growth mechanism of these cavities.

IV.4. Formation and Failure of the Fibrillar Structure

A very interesting aspect of the debonding mechanisms of the PSA's is the transition from a structure of cavities initially formed at the interface between the probe and the film into a fibrillar structure. The formation of the structure can be described as follows: During the stage where the measured total force decreases, the load-bearing area decreases. However, when the thickness of the walls between the cavities decreases to 50 – 100 μm, the cavities stop growing in the plane of the film and grow mainly perpendicularly to it. The nominal force remains relatively constant, therefore implying that the local stress remains relatively constant as well. Eventually, the local stress on the walls increases again, due to a strain-hardening mechanism, and failure occurs, either:

- at the interface between the probe and the film (in this case the foot of the wall detaches from the probe)
- cohesively in the middle of the fibril

– adhesively at the glass probe interface (in this case a new cavity nucleates at the glass/film interface and propagates rapidly over the whole interface)

Let us examine first the conditions for the transition from cavities to fibrils. If the surface of the probe is kept constant, the transition is controlled by the rheology of the adhesive and by the contact time. From the analysis of Figure 15b, one notes that, for the PEHA adhesive, the fibrillar structure no longer forms for low values of $a_T V$. This is due to the extremely easy propagation of the nucleated voids in the plane of the film so that the film essentially dewets from the surface.

On the other hand, for the PEHA-AA, the fibrillar structure no longer occurs for the high values of $a_T V$. In this case, the debonding occurs by the formation of cracks which propagate in a completely unstable manner from one cavity to another. One cannot observe the growth of the cavities and the critical distance of 50 – 100 μm between cavities is never observed.

Apparently, there is a time-temperature window where fibrillation can occur. If the relaxation times are too short, the polymer behaves like a liquid and does not form fibrils, while if the relaxation times are too long, the necessary disentanglement to form fibrils does not occur. The presence of acrylic acid shifts the fibrillation window towards higher temperatures and lower debonding rates. This result is in agreement with an empirical model correlating rheology and tack properties which has been recently proposed [40]. It may appear surprising that at low temperatures PEHA-AA does not fibrillate while both PEHA and PEHA-AA have a very similar shear modulus in that regime (see Fig. 1). The difference in behavior can, therefore, only be attributed to a significant difference in the non-linear elongational properties which should play an important role in the formation of fibrils. Preliminary experiments in elongation are in qualitative agreement with this conclusion.

Once the fibrillar structure has formed, *i.e.*, a distinctive plateau appears in the stress – strain curve, it is important to understand which factors will influence the stability of the fibrillar structure and its eventual failure, either by debonding of the fibrils from the probe or from the glass, or by cohesive fracture of the fibrils. An increased

fibrillar stability will result in a higher value for the maximum deformation measured with the stress–strain curve. In Figure 25 we show the maximum deformation of the fibrils, ε_{max}, as a function of $a_T V$ for both polymers. This parameter shows a distinctively different behavior for the PEHA and PEHA-AA, reflecting the very different elongational properties of the two polymers. As shown on Figure 25b, in the case of the PEHA-AA, the maximum appears to have a

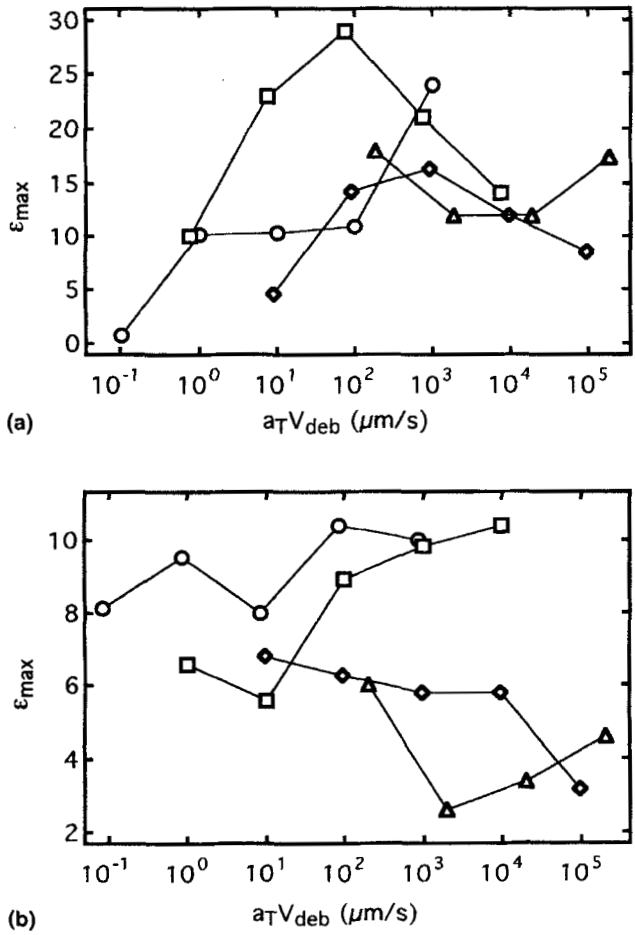

FIGURE 25 Maximum elongation of the fibrils ε_{max} as a function of $a_T V$ at a reference temperature of 20°C for the (a) PEHA and (b) PEHA-AA (–○– 50°C, –□– 20°C, –◇– 0°C, –△– –20°C).

transition between a high temperature behavior and a low temperature behavior, consistent with the change in mechanism from fibrillar to brittle. In the high temperature regime, it is weakly rate-dependent and the maximum extension ratios do not exceed 10.

By contrast, the value of ε_{max} for PEHA has a distinctive rate dependence at 20°C and 50°C and is rather rate independent for $T = -20$°C and 0°C. This difference is somewhat puzzling at first since the adhesive fails in a fibrillar way at all temperatures. Furthermore, the maximum extension ratios are much higher than for the PEHA-AA.

Finally, for both polymers the maximum extension ratio does not appear to obey a time-temperature superposition. This is not surprising since one expects the maximum elongation to be controlled by the nonlinear elongational properties and by the interactions with the surface.

These observations can be interpreted as follows:

The presence of acrylic acid strongly hinders the disentanglement of the polymer chains (consistent with the increase in the long relaxation times seen in shear on Fig. 1). In that case, the fibrils will extend to a value close to the maximum natural draw ratio of the polymer. For a weakly-entangled polymer such as poly(2-ethylhexyl acrylate) a value of 10 is not unreasonable [41]. In this case, a strong strain hardening would occur when the draw ratio is reached, causing a debonding of the fibril from the surface of the probe.

On the other hand, for the PEHA the disentanglement is much easier, so that the maximum extension of the fibrils is mostly controlled by the creep of the polymer. This results in higher extension ratios than for the PEHA-AA. The existence of a clear maximum in ε_{max} with a_TV for $T = 20$°C, on the other hand, is consistent with a failure when a critical stress is reached: for low values of a_TV, the polymer will disentangle before it reaches the critical stress for catastrophic failure, while for high values of a_TV, the fibrils will fail when they reach the critical stress (an event which occurs at lower values of ε with increasing V).

It is difficult to understand these differences without a detailed analysis of the entire debonding mechanism and, in particular, of the failure mode. An interesting first observation is that for both polymers the failure mode changes from adhesive/probe to cohesive and then to

adhesive/glass for increasing temperatures and decreasing debonding rates.

However, one does not expect the interactions between the surface and the polymer to change much with temperature and certainly not with debonding rate. Therefore, we should look towards a rheological explanation for these transitions. Once the cavities are formed and have reached their "equilibrium size", *i.e.*, at the beginning of the plateau, the walls between the cavities will elongate in the direction parallel to the tensile stress. This will occur by a decrease of the wall thickness but also by a flow of polymer from one or the other of the feet of the wall. In the late stages of the elongation of these walls, the flow can also occur from the foot close to the glass surface as shown on Figure 26. If the continuous layer of polymer at the glass surface becomes very thin, the tensile stress distribution at the glass/polymer interface becomes markedly non-uniform, higher underneath the walls themselves and lower between them. This high stress can, in turn, nucleate cavities at the glass/polymer interface. The local stress concentration caused by the walls will cause these cavities to turn into cracks and eventually the whole polymer film debonds from the glass surface, even though the initial cavities were nucleated at the probe/polymer interface. This mechanism is predominantly observed for the PEHA polymer and explains why the maximum fibril elongation obeys a criterion of a critical stress: it is, indeed, the critical stress to nucleate a cavity at the glass/film interface which causes the failure.

For this mechanism to occur, one needs some strain hardening of the walls but maybe, more importantly, also flow of polymer from the glass side of the wall's foot into the wall itself to create a local stress concentration at the glass/polymer interface. This flow is favored by a higher temperature and a lower debonding rate and hindered by the presence of acrylic acid.

An important question, then, is why does the wall not debond from the probe? In fact, the small asperities on the rough probe act as mechanical anchoring points. If one uses a polished metal probe the failure mode for the PEHA is bi-adhesive, *i.e.*, large sections of the contact surface debond from the probe and other large sections debond from the glass. This implies that, for the rough-probe case, the difference in interfacial interactions is not important but it is the difference in roughness which causes the preferential debonding from the glass.

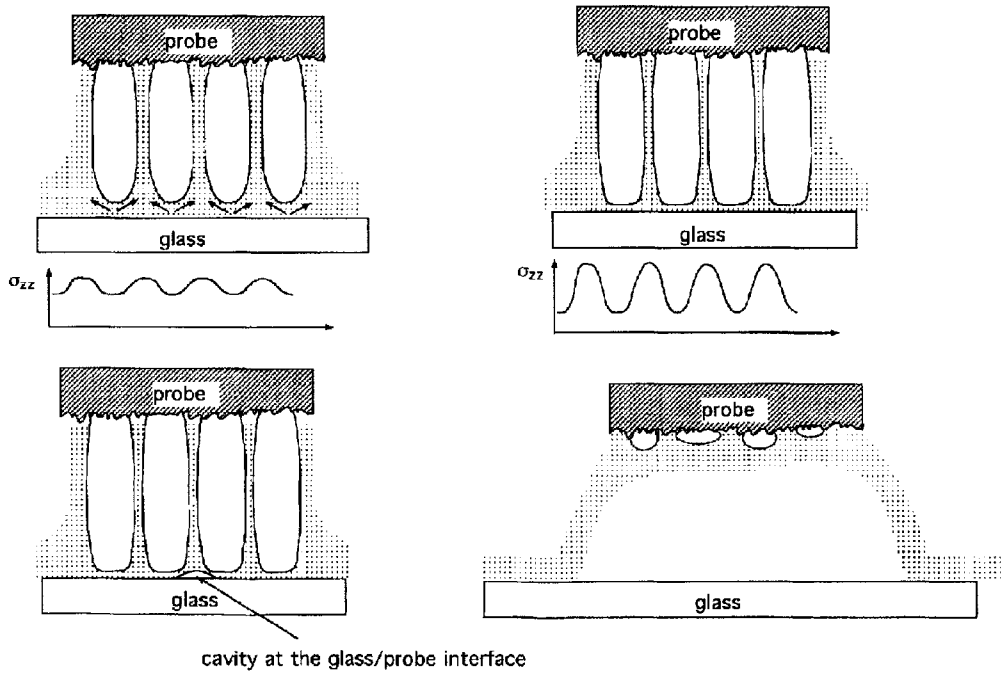

FIGURE 26 Schematics of the cavitation process and the late-stage debonding when the locus of failure is at the glass/film interface.

At the opposite end of the temperature/rate spectrum is the transition from adhesive/probe to cohesive. In this regime, the flow from the foot of the wall is difficult and once the wall is formed it grows predominantly by wall thinning. In this case, the local tensile stress at the probe/polymer interface is much higher than at the glass/polymer interface where it is averaged out and the failure occurs either cohesively by fracture of the wall in its thinnest section, or adhesively on the side where the original cavities were nucleated. For these conditions one expects the fibril to fail at a critical strain and it is indeed observed for the PEHA-AA polymer and for the PEHA polymer at $-20°C$ and $0°C$ where ε_{max} is about $10-15$ and relatively independent of the debonding rate. Presumably one needs some strain hardening of the wall to debond from the probe surface and a lower temperature results in a bigher stress. In this case the presence of acrylic acid significantly enhances the strain hardening and favors the adhesive debonding from the probe surface.

V. CONCLUSIONS

The *in-situ* observation of the microscopic mechanisms taking place during the debonding of two model acrylic PSA's in a probe tack experiment has provided novel information on the mechanisms of formation of a fibrillar structure, which is crucial to the good performance of a PSA. In all cases investigated, the initial stages of the debonding are mainly controlled by the very strong confinement imposed on the adhesive by the probe tack geometry using a flat probe. The negative hydrostatic pressure imposed in the initial stages of the debonding causes the appearance of cavities at the interface between the probe and the film.

The cavities appear preferentially at defects (presumably microscopic air pockets trapped during the contact stage) and the maximum stress experimentally observed corresponds to the widespread nucleation of these cavities over all of the probe surface. For our model adhesives, the maximum stress was controlled mainly by the elastic shear modulus of the adhesive, except for the PEHA polymer at the higher temperatures, where it was controlled by both the shear modulus of the adhesive and the interactions at the interface.

The cavities do not appear at the center of the probe first but are nucleated in a random fashion over the whole surface implying, therefore, that the negative hydrostatic stress is fairly homogeneous over the surface of the probe. This result can be used to estimate the Poisson's ratio or the bulk modulus of the polymer.

After the cavities are nucleated, they grow laterally on the probe surface like interfacial cracks in a viscoelastic medium. The kinetics of this growth are very sensitive to the interactions between the surface of the probe and the film. Eventually, the walls between the cavities stabilize to a size of $50-100\,\mu m$ and grow in the direction of the applied tensile stress to form a fibrillar structure. The transition from a cavitated to a fibrillar structure is only possible in a time-temperature window which appears to be controlled mainly by the long relaxation times of the polymer.

At experimental times longer than the useful window, we observe a liquid-like behavior of dewetting under stress but no formation of stable fibrils, while, at shorter times, we observe a coalescence of the cavities into an interfacial crack which propagates catastrophically.

If the fibrillar structure is formed, the maximum elongation which is observed is controlled by a criterion of maximum strain. For the PEHA-AA polymer, this critical strain is not strongly influenced by the debonding rate, reflecting the fact that, presumably, negligible disentanglement occurs in the fibril due to the very long relaxation times introduced by the presence of acrylic acid. For the PEHA, on the other hand, this maximum strain varies with debonding rate and temperature and reflects the substantial flow occurring inside the fibril. A peculiar mechanism of debonding from the substrate is observed at high temperature for the PEHA and is due to the nucleation and rapid growth of a cavity on the flat glass surface. In that regime, the maximum extension of the fibrils is controlled by a maximum stress criterion and exhibits, therefore, a maximum with debonding rate.

Acknowledgements

We are grateful to Denis Melot and François Court of ELF-Atochem for providing the model PSA's and for helpful discussions. The sanding of the probes and the characterization of their roughness were kindly done by

Michel Degrange and Denis Bouter of the Université Paris V and the finite element calculations were done by A. Burr of the ESPCI. We also thank K. R. Shull for stimulating discussions and comments on the early version of the manuscript and A. Zosel for providing us with preprints of his work prior to publication.

References

[1] Zosel, A., *Advances in Pressure Sensitive Adhesive Technology* **1**, 92 (1992).
[2] *Handbook of Pressure Sensitive Adhesive Technology* **1**, Satas, D., Ed. (Van Nostrand Reinhold, New York, 1989).
[3] Chuang, H. K., Chiu, C. and Paniagua, R., *Adhesives Age* **18** (September 1997).
[4] Johnson, K. L., Kendall, K. and Roberts, A. D., *Proc. Royal Society of London, series A: Mathematical and Physical Sciences* **A324**, 301 (1971).
[5] Shull, K. R., Ahn, D., Chen, W. L., Mowery, C. L. and Crosby, A. J., *Macromolecular Chemistry and Physics* **199**, 489 (1998).
[6] Maugis, D. and Barquins, M., *J. Physics D: Applied Physics* **11**, 1989 (1978).
[7] Maugis, D., *J. Mater. Sci.* **20**, 3041 (1985).
[8] Barquins, M. and Maugis, D., *J. Adhesion* **13**, 53 (1981).
[9] Ondarçuhu, T., *Journal de Physique II* **7**, 1893 (1997).
[10] de Gennes, P. G., *Langmuir* **12**, 4497 (1996).
[11] Xu, D. B., Hui, C. Y. and Kramer, E. J., *J. Appl. Physics* **72**, 8 (1992).
[12] Hui, C. Y., Xu, D. B. and Kramer, E. J., *J. Appl. Physics* **72**, 3294 (1992).
[13] Creton, C. and Leibler, L., *J. Polym. Sci.: Part B: Polymer Physics* **34**, 545 (1996).
[14] Zosel, A., *J. Adhesion Sci. Technol.* **11**, 1447 (1997).
[15] Creton, C., in *Processing of Polymers* **18**, 1st ed., Meijer, H. E. H., Ed. (VCH, Weinheim, 1997), p. 707.
[16] Zosel, A., *J. Adhesion* **30**, 135 (1989).
[17] Kaelble, D. H., *Trans. Society of Rheology* **9**, 135 (1965).
[18] Urahama, Y., *J. Adhesion* **31**, 47 (1989).
[19] Derail, C., Allal, A., Marin, G. and Tordjeman, P., *J. Adhesion* **61**, 123 (1997).
[20] Benyahia, L., Verdier, C. and Piau, J. M., *J. Adhesion* **62**, 45 (1997).
[21] Ferguson, J., Reilly, B. and Granville, N., *Polymer* **38**, 795 (1997).
[22] Good, R. J. and Gupta, R. K., *Adhesion* **26**, 13 (1988).
[23] Zosel, A., *J. of Adhesion* **34**, 201 (1991).
[24] Zosel, A., to be published in *Int. J. Adhesion and Adhesives.*
[25] Kaelble, D. H., *Trans. Society of Rheology* **15**, 275 (1971).
[26] Zhang Newby, B. M. and Chaudhury, M. K., *Langmuir* **13**, 1805 (1997).
[27] Ferry, J. D., *Viscoelastic Properties of Polymers* **1**, 3rd ed. (Wiley, New York, 1980).
[28] Ahn, D., Thesis, Northwestern University, 1997.
[29] Hammond, F. H., *ASTM Special Technical Publication* **360**, 123 (1964).
[30] Zosel, A., *Colloid and Polym. Sci.* **263**, 541 (1985).
[31] Kim, H. J. and Mizumachi, H., *J. Adhesion* **49**, 113 (1995).
[32] Aubrey, D. W. and Ginosatis, S., *J. Adhesion* **12**, 189 (1981).
[33] Gent, A. N. and Wang, C., *J. Mater. Sci.* **26**, 3392 (1991).
[34] Gent, A. N. and Lindley, P. B., *Proc. Royal Society London series A: Mathematical and Physical Sciences* **249A**, 195 (1958).
[35] Gent, A. N., *Rubber Chem. Technol.* **67**, 549 (1994).
[36] Ganghoffer, J. F. and Gent, A. N., *J. Adhesion* **48**, 75 (1995).
[37] Ganghoffer, J. F. and Schultz, J., *J. Adhesion* **55**, 285 (1996).

[38] Gent, A. N. and Tompkins, D. A., *J. Polym. Sci. Part A-2 Polym. Physics* **7**, 1483 (1969).
[39] Creton, C. *et al.*, to be published.
[40] Chang, E. P., *J. Adhesion* **34**, 189 (1991).
[41] Kramer, E. J. and Berger, L. L., *Adv. Polym. Sci.* **91/92**, 1 (1990).